THE ASTROPHYSICAL JOURNAL, 437:742–769, 1994 December 20

HYDRODYNAMICS OF ROTATING STARS AND CLOSE BINARY INTERACTIONS: COMPRESSIBLE ELLIPSOID MODELS

DONG LAI[1]
Center for Radiophysics and Space Research, Cornell University, Ithaca, NY 14853;
dong@tapir.caltech.edu
FREDERIC A. RASIO[2]
Institute for Advanced Study, Olden Lane, Princeton, NJ 08540; rasio@guinness.ias.edu
AND
STUART L. SHAPIRO[3]
Center for Radiophysics and Space Research, Cornell University, Ithaca, NY 14853
Received 1994 April 4; accepted 1994 June 20

ABSTRACT

We develop a new formalism to study the dynamics of fluid polytropes in three dimensions. The stars are modeled as compressible ellipsoids, and the hydrodynamic equations are reduced to a set of ordinary differential equations for the evolution of the principal axes and other global quantities. Both viscous dissipation and the gravitational radiation reaction are incorporated. We establish the validity of our approximations and demonstrate the simplicity and power of the method by rederiving a number of known results concerning the stability and dynamical oscillations of rapidly rotating polytropes. In particular, we present a generalization to compressible fluids of Chandrasekhar's classical results for the secular and dynamical instabilities of incompressible Maclaurin spheriods. We also present several applications of our method to astrophysical problems of great current interest, such as the tidal disruption of a star by a massive black hole, the coalescence of compact binaries driven by the emission of gravitational waves, and the development of instabilities in close binary systems.

Subject headings: binaries: close — hydrodynamics — instabilities — stars: oscillations — stars: rotation

1. INTRODUCTION

In a series of recent papers (Lai, Rasio, & Shapiro 1993a, b, 1994a, b, hereafter LRS1–LRS4 or collectively LRS), we have developed a new analytic method to calculate ellipsoidal figures of equilibrium both for a single rotating polytrope and for polytropes in binary systems. Our approach is based on the use of an energy variational principle to construct approximate equilibrium solutions and to determine their dynamical and secular stability. In addition to providing compressible generalizations for all the classical incompressible solutions (Chandrasekhar 1969, hereafter Ch69), our method can also be applied to more general models of binary systems where the stellar masses, radii, spins, entropies, and polytropic indices are all allowed to vary independently for each component. As a result, we were able to study the equilibrium and stability properties of many different types of fairly realistic binary models (see especially LRS4).

We have used the method to explore the implications of instabilities for the coalescence of close binary systems (LRS2, LRS3). Of particular importance currently are coalescing neutron star binaries, which are the primary targets for the detection of gravitational waves by LIGO (Abramovici et al. 1992; LRS3). In our previous papers we have studied these systems by considering equilibrium sequences of binary configurations, treating the binary separation r as a dynamical variable but with all other variables assuming their equilibrium values. This is adequate to capture the essential features of the evolution, but does not provide quantitatively accurate results when the orbital evolution takes place on a timescale comparable to the internal hydrodynamic timescale. The purpose of the present paper is to extend our formalism and develop a fully dynamical theory for the evolution of compressible ellipsoids.

Detailed studies of hydrodynamic interactions between stars normally require large-scale numerical simulations in three dimensions (see, e.g., Lai, Rasio, & Shapiro 1993c; Rasio & Shapiro 1991, 1994). These simulations demand extensive computational resources and cannot be used to cover a large parameter space. In our treatment, we replace the infinite number of degrees of freedom in a fluid system by a small number of variables specifying the essential geometric and kinematic properties of the system. The dynamics is then described approximately by a set of ordinary differential equations (ODEs) for the time evolution of these variables. This represents an enormous simplification. However, for many problems, useful insights and even reliable quantitative results can be obtained using such an approach. The simplicity of a formulation in terms of ODEs allows for extensive coverage of the parameter space. In addition, we can follow the evolution of a system over a large number of dynamical times without having to worry about excessive computational time or about the growth of numerical errors. This advantage is crucial for studying the secular evolution of a system on a dissipative timescale while still allowing for dynamical processes. A distinctive example is the

[1] Current address: Theoretical Astrophysics, California Institute of Technology, Pasadena, CA 91125.
[2] Hubble Fellow.
[3] Departments of Astronomy and Physics, Cornell University.

coalescence of binary neutron stars, which begins as a very slow orbital decay driven by the emission of gravitational waves but ends in a rapid hydrodynamic merging of the two stars after the stability limit has been reached (LRS3; Rasio & Shapiro 1994).

In the incompressible limit, the dynamics of an isolated ellipsoid was first formulated by Lebovitz (1966; see also Ch69, chap. 4). This so-called Riemann-Lebovitz formulation of the problem forms the basis of many subsequent studies and astrophysical applications of ellipsoidal models. In particular, the effects of fluid viscosity and gravitational radiation reaction on the stability of a rapidly rotating star were investigated by Chandrasekhar (1970), Press & Teukolsky (1973), Miller (1974), and Detweiler & Lindblom (1977). The Riemann-Lebovitz equations have also been used to study the gravitational collapse of rotating stars and the resulting gravitational radiation by relaxing the assumption of incompressibility and incorporating a polytropic equation of state while still assuming a homogeneous density profile (see Shapiro 1979 and references therein). Nduka (1971) has studied the dynamics of an incompressible ellipsoid in a parabolic orbit around a fixed point mass.

For compressible systems, Carter & Luminet (1983, 1985) have developed a dynamical theory of an affine stellar model in the context of tidal interactions with a massive black hole. Kochanek (1992a, b) has used the method to study the tidal capture of a polytrope by a point mass and the coalescence of two polytropes in a close binary. In the affine model, the fluid compressibility is treated under the assumption that the surfaces of constant density remain self-similar ellipsoids. Our dynamical model for compressible ellipsoids is essentially equivalent to the affine model (cf. LRS1), but our formulation of the problem is quite different and our dynamical equations more closely resemble the Riemann-Lebovitz equations in the incompressible limit. In contrast to previous studies, we present a completely general formulation for isolated stars and for a star on a bound or unbound trajectory around a point mass. We incorporate both viscosity and gravitational radiation reaction as possible dissipation mechanisms. Our formulation makes explicit use of global quantities such as the total angular momentum and fluid circulation which are conserved in the absence of dissipation. This greatly simplifies the description of many dynamical processes, and we feel that this simplification has not been fully appreciated in previous studies based on the affine model.

The main purpose of this paper is to formulate general dynamical equations for compressible ellipsoids and to present a small survey of astrophysical applications. We wish to illustrate how these general equations can be used to tackle a variety of multidimensional hydrodynamic problems of great current interest. The dynamical equations for an isolated ellipsoid supported by a polytropic equation of state are derived in § 2, where our general assumptions are also presented (§ 2.1). Many of the expressions derived in § 2 can be readily transported to more general situations. In § 3 we consider the dynamical stability and oscillations of a single rotating polytrope. In § 4 we incorporate viscous dissipation and gravitational radiation reaction into the dynamical equations, and we study the secular evolution of isolated rotating stars. In § 5 the dynamical equations derived in § 2 for single stars are generalized to a binary system (either bround or unbound) consisting of a polytrope and a point mass. The dynamical stability of general Roche-Riemann binary models is considered in § 6. In § 7 we study tidal encounters of a star with a massive body, and we compare our results with those of linear perturbation theory as well as previous nonlinear calculations. In § 8 we consider the evolution of binary systems driven by viscous dissipation. In § 9 we incorporate gravitational radiation reaction in our treatment of binaries, and we study the orbital evolution driven by gravitational radiation.

2. DYNAMICAL EQUATIONS FOR SINGLE STARS: RIEMANN-S ELLIPSOIDS

In this section we derive the equations of motion for an isolated compressible Riemann-S ellipsoid. Our equations represent a generalization of the Riemann-Lebovitz equations, which only apply to an incompressible fluid (Ch69, chap. 4).

2.1. *Assumptions*

Throughout this paper we adopt a polytropic equation of state for the fluid,

$$P = K\rho^{1+1/n} . \tag{2.1}$$

Our basic assumptions concerning the interior structure of the star can be summarized as follows (see LRS1 for more details). We assume that the surfaces of constant density can be represented approximately by *self-similar ellipsoids*. The geometry is then completely specified by the three principal axes of the outer surface. Furthermore, we assume that the density profile $\rho(m)$ inside each star, when m is the mass interior to an isodensity surface, is identical to that of a *spherical* polytrope with the same volume. In the reference frame comoving with the star's center of mass, the velocity field of the fluid is modeled as a linear superposition of three components: (1) a rigid rotation of the ellipsoidal *figure*; (2) an internal fluid circulation with *uniform vorticity*; and (3) an ellipsoidal expansion or contraction (see eqs. [2.3] and [2.4] below).

Under these assumptions, the number of internal degrees of freedom for each star is reduced to nine in general: the three principal axes, a_1, a_2, a_3 of the outer surface; the three components of the angular velocity of the ellipsoidal figure, Ω_1, Ω_2, Ω_3; and the three components of the vorticity, ζ_1, ζ_2, ζ_3. We shall further restrict ourselves to the cases where both the angular velocity and the vorticity are parallel to one of the principal axes, here taken to be the z or a_3 axis by convention. This choice corresponds to the Riemann ellipsoids of type S (Ch69). As we show in § 2.2, under these conditions the exact hydrodynamic equations (the Euler and Navier-Stokes equations, with and without the gravitational radiation reaction) are replaced by a set of ODEs for the time evolution of the principal axes a_1, a_2, a_3, the angular velocity of the ellipsoidal figure $\Omega = \Omega_3$, and the angular frequency of the internal circulation $\Lambda \propto \zeta_3$, (cf. LRS1, § 5.1).

As we noted in § 1, our model is formally equivalent to the affine model developed extensively by Carter & Luminet (1985; see also Luminet & Carter 1986). In the incompressible limit ($n = 0$), both models can be obtained equivalently by imposing fixed holonomic constraints on the system, requiring the fluid surface to be ellipsoidal and the fluid velocity to be a linear function of coordinates. This is known as the Dirichlet problem (see Ch69, chap. 4). In the $n = 0$ limit, our dynamical equations reduce explicitly to the equations obtained in the Riemann-Lebovitz formulation of the Dirichlet problem (Ch69, § 27). For a single isolated star with $n = 0$, the solutions we derive represent *exact* solutions of the true hydrodynamic equations. For $n \neq 0$, our solutions are only approx-

imate, since the isodensity surfaces can no longer be exactly ellipsoidal, and the velocity field of the fluid cannot be described exactly by a linear function of coordinates (see Ipser & Managan 1981 for a formal proof). For binary systems, our solutions are always approximate because we truncate the gravitational interaction to quadrupole order (see § 5 below).

Clearly, our formalism cannot be applied to hydrodynamic processes such as stellar collisions that are violet enough to disrupt a star completely or to produce significant shock heating. Even for dynamical processes that are not very disruptive, our treatment allows us to follow only a small subset of the many degrees of freedom that may be important. This is especially true for compressible systems, which have typically many more important degrees of freedom than incompressible systems. Consider, for example, small nonradial oscillations of a star (see, e.g., Cox 1980). For $n = 0$, only the f-modes of oscillation exist. But when $n \neq 0$, there are many additional p-modes and possibly also g-modes of oscillation, corresponding to nonellipsoidal disturbances of the star. Such nonellipsoidal motions cannot be described at all within our simplified treatment. Even for $n = 0$, an ellipsoidal model can only represent the $l = 2$, quadrupolar f-modes of oscillation. These modes often dominate the response of a star to tidal perturbations by passing objects (see Kochanek 1992a and § 7 below), but they are not sufficient for a complete description of the dynamical response (cf. Press & Teukolsky 1977).

2.2. *Derivation of the Dynamical Equations*

Let $\boldsymbol{e}_1$, $\boldsymbol{e}_2$, and $\boldsymbol{e}_3$ be the basis unit vectors along the instantaneous directions of the principal axes of the ellipsoid, with $\boldsymbol{e}_3$ along the rotation axis (we refer to this as the *body frame*). In the inertial frame, the velocity field $\boldsymbol{u}$ inside the ellipsoid can be written as

$$\boldsymbol{u} = \boldsymbol{u}_s + \boldsymbol{u}_e \,. \tag{2.2}$$

Here $\boldsymbol{u}_s$ is the velocity field of an equilibrium Riemann-S ellipsoid,

$$\boldsymbol{u}_s = \left(\frac{a_1}{a_2}\Lambda - \Omega\right) x_2 \boldsymbol{e}_1 + \left(-\frac{a_2}{a_1}\Lambda + \Omega\right) x_1 \boldsymbol{e}_2 \,, \tag{2.3}$$

where Ω is the angular velocity of the ellipsoidal figure and Λ is the angular frequency of the internal fluid circulation (cf. LRS1, § 5.1). For nonequilibrium configurations, we add the velocity $\boldsymbol{u}_e$ describing an ellipsoidal expansion or contraction of the star,

$$\boldsymbol{u}_e = \frac{\dot{a}_1}{a_1} x_1 \boldsymbol{e}_1 + \frac{\dot{a}_2}{a_2} x_2 \boldsymbol{e}_2 + \frac{\dot{a}_3}{a_3} x_3 \boldsymbol{e}_3 \,. \tag{2.4}$$

The kinetic energy is then given by

$$T = \int d^3x \tfrac{1}{2}\rho \boldsymbol{u}^2 = T_s + T_e \,. \tag{2.5}$$

Here T_s is the "spin" kinetic energy (rotation and internal circulation of the fluid; cf. LRS1, eq. [5.6]),

$$T_s = \tfrac{1}{2} I(\Lambda^2 + \Omega^2) - \tfrac{2}{5}\kappa_n M a_1 a_2 \Lambda\Omega \,, \tag{2.6}$$

where I is the moment of inertia,

$$I = \tfrac{1}{5}\kappa_n M(a_1^2 + a_2^2) \,, \tag{2.7}$$

κ_n is a structure constant depending on the polytropic index (numerical values are given in LRS1, Table 1), and T_e is the kinetic energy associated with the expansion or contraction,

$$T_e = \tfrac{1}{10}\kappa_n M(\dot{a}_1^2 + \dot{a}_2^2 + \dot{a}_3^2) \,. \tag{2.8}$$

The total internal energy U of the fluid is given by

$$U = \int \frac{nP}{\rho}\, dm = k_1 K \rho_c^{1/n} M \,, \tag{2.9}$$

where k_1 is a constant depending on the polytropic index and ρ_c is the central density, equal to that of a spherical polytrope with the same mass and volume in our approximation (see LRS1, § 2.1). The self-gravitational potential energy is given by

$$W = -\frac{3}{5-n}\frac{GM^2}{R} f \,, \tag{2.10}$$

where $R \equiv (a_1 a_2 a_3)^{1/3}$ is the mean radius of the ellipsoid, and

$$f = \frac{\mathscr{I}}{2R^2} \,, \qquad \text{with} \qquad \mathscr{I} = A_1 a_1^2 + A_2 a_2^2 + A_3 a_3^2 \tag{2.11}$$

($f = 1$ for spherical configurations). The dimensionless index symbols A_i are defined as in Ch69 (§ 17).

The Lagrangian governing the dynamics of the ellipsoid can now be written as

$$L(q_i; \dot{q}_i) = T - U - W \,, \tag{2.12}$$

where $\{q_i\} = \{a_1, a_2, a_3, \phi, \psi\}$, and $\{\dot{q}_i\} = \{\dot{a}_1, \dot{a}_2, \dot{a}_3, \Omega, \Lambda\}$ (we have introduced angles ϕ and ψ such that $\dot{\phi} = \Omega$ and $\dot{\psi} = \Lambda$). The dynamical equations are obtained from the Euler-Lagrange equations

$$\frac{d}{dt}\frac{\partial L}{\partial \dot{q}_i} = \frac{\partial L}{\partial q_i} . \tag{2.13}$$

Using the relation (Ch69, chap. 2)

$$\frac{\partial \mathscr{I}}{\partial a_i} = \frac{1}{a_i}(\mathscr{I} - a_i^2 A_i) , \tag{2.14}$$

equation (2.13) for $q_i = a_1$ can be written as

$$\frac{1}{2}\kappa_n M\ddot{a}_1 = \frac{1}{5}\kappa_n M a_1(\Omega^2 + \Lambda^2) - \frac{2}{5}\kappa_n M a_2 \Omega\Lambda + \frac{k_1 M}{n a_1}\frac{P_c}{\rho_c} - \frac{2\pi}{5-n} MG\bar{\rho} a_1 A_1 , \tag{2.15}$$

where $\bar{\rho} = 3M/(4\pi R^3)$ is the mean density. Equations for a_2 and a_3 can be similarly obtained. For $q_i = \phi$ and ψ, equation (2.13) yields the conservation laws for angular momentum and circulation,

$$\frac{dJ_s}{dt} = 0 , \qquad \frac{d\mathscr{C}}{dt} = 0 , \tag{2.16}$$

where J_s is the angular momentum,

$$J_s = \frac{\partial L}{\partial \Omega} = I\Omega - \frac{2}{5}\kappa_n M a_1 a_2 \Lambda , \tag{2.17}$$

and $\mathscr{C}$ is the fluid circulation (cf. LRS1),

$$\mathscr{C} = \frac{\partial L}{\partial \Lambda} = I\Lambda - \frac{2}{5}\kappa_n M a_1 a_2 \Omega . \tag{2.18}$$

The complete set of dynamical equations can be rewritten in the form

$$\ddot{a}_1 = a_1(\Omega^2 + \Lambda^2) - 2a_2\Omega\Lambda - \frac{2\pi G}{q_n} a_1 A_1 \bar{\rho} + \left(\frac{5k_1}{n\kappa_n}\right)\frac{P_c}{\rho_c}\frac{1}{a_1} , \tag{2.19}$$

$$\ddot{a}_2 = a_2(\Omega^2 + \Lambda^2) - 2a_1\Omega\Lambda - \frac{2\pi G}{q_n} a_2 A_2 \bar{\rho} + \left(\frac{5k_1}{n\kappa_n}\right)\frac{P_c}{\rho_c}\frac{1}{a_2} , \tag{2.20}$$

$$\ddot{a}_3 = -\frac{2\pi G}{q_n} a_3 A_3 \bar{\rho} + \left(\frac{5k_1}{n\kappa_n}\right)\frac{P_c}{\rho_c}\frac{1}{a_3} , \tag{2.21}$$

$$\frac{d}{dt}(a_1\Omega - a_2\Lambda) = -\dot{a}_1\Omega + \dot{a}_2\Lambda , \tag{2.22}$$

$$\frac{d}{dt}(-a_2\Omega + a_1\Lambda) = \dot{a}_2\Omega - \dot{a}_1\Lambda , \tag{2.23}$$

where $q_n \equiv \kappa_n(1 - n/5)$. Rather than using equations (2.22) and (2.23) as such, we shall use the equivalent pair

$$\dot{\Omega} = \left(\frac{a_2}{a_1} - \frac{a_1}{a_2}\right)^{-1}\left[2\left(\frac{\Omega}{a_2} + \frac{\Lambda}{a_1}\right)\dot{a}_1 - 2\left(\frac{\Omega}{a_1} + \frac{\Lambda}{a_2}\right)\dot{a}_2\right] , \tag{2.24}$$

$$\dot{\Lambda} = \left(\frac{a_2}{a_1} - \frac{a_1}{a_2}\right)^{-1}\left[2\left(\frac{\Omega}{a_1} + \frac{\Lambda}{a_2}\right)\dot{a}_1 - 2\left(\frac{\Omega}{a_2} + \frac{\Lambda}{a_1}\right)\dot{a}_2\right] . \tag{2.25}$$

In addition to the conservation of total angular momentum and circulation (eqs. [2.17] and [2.18]), it is easy to check that the total energy is also conserved, i.e.,

$$\mathscr{E} = \mathscr{E}_s = T + U + W = \text{constant} . \tag{2.26}$$

For $\ddot{a}_i = 0$, one can verify that equations (2.19)–(2.21) reduce to the equilibrium equations for Riemann-S ellipsoids derived in LRS1 (§ 5.1).

2.3. *The Pressure Term*

To implement the dynamical equations in numerical integrations, it is convenient to express the pressure term $(5k_1 P_c)/(n\kappa_n \rho_c)$ in terms of R_0, M, and other dynamical variables, when R_0 is the radius of a nonrotating spherical polytrope of the same mass M and

polytropic constant K. This is done as follows. Since $P_c/\rho_c = K\rho_c^{1/n} \propto R^{-3/n}$, we can write

$$\frac{5k_1}{n\kappa_n}\frac{P_c}{\rho_c} = C_n R^{-3/n}, \tag{2.27}$$

where C_n is a constant depending only on n, K, M. We can obtain the value of C_n by considering a single, nonrotating spherical polytrope in equilibrium. For such a configuration, equations (2.19)–(2.21) become

$$0 = -\frac{2\pi G}{q_n} R_0 A_1 \bar{\rho}_0 + C_n R_0^{-3/n}\frac{1}{R_0}. \tag{2.28}$$

As $A_1 = \frac{2}{3}$ for a sphere, we get

$$C_n = \frac{GM}{q_n} R_0^{3/n-1}. \tag{2.29}$$

Therefore, in equations (2.19)–(2.21), we can use

$$\frac{5k_1}{n\kappa_n}\frac{P_c}{\rho_c} = \frac{GM}{q_n R_0}\left(\frac{R_0}{R}\right)^{3/n} \qquad (n \neq 0). \tag{2.30}$$

Expression (2.30) is obviously not valid in the incompressible case. For $n \to 0$, $k_1/n \to \frac{2}{5}$ and $\kappa_n \to 1$, so that

$$\frac{5k_1}{n\kappa_n}\frac{P_c}{\rho_c} = \frac{2P_c}{\rho_c} \qquad (n = 0). \tag{2.31}$$

To evaluate $2P_c/\rho_c$ in this limit, we need to use the incompressible condition

$$a_1 a_2 a_3 = R_0^3 = \text{constant}, \tag{2.32}$$

which gives

$$\frac{\dot{a}_1}{a_1} + \frac{\dot{a}_2}{a_2} + \frac{\dot{a}_3}{a_3} = 0. \tag{2.33}$$

Now adding (eq. [2.19])/a_1, (eq. [2.20])/a_2 and (eq. [2.21])/a_3, and using the above expression, we get

$$\frac{5k_1}{n\kappa_n}\frac{P_c}{\rho_c} = \frac{2P_c}{\rho_c} = \left(\sum_i \frac{1}{a_i^2}\right)^{-1}\left[\sum_i\left(\frac{\dot{a}_i}{a_i}\right)^2 - 2(\Omega^2+\Lambda^2) + 2\Omega\Lambda\left(\frac{a_2}{a_1}+\frac{a_1}{a_2}\right) + 4\pi G\bar{\rho}\right] \qquad (n = 0), \tag{2.34}$$

where we have used $A_1 + A_2 + A_3 = 2$. From equation (2.30), we see that the internal energy (2.9) can also be written as

$$U = k_1\frac{P_c}{\rho_c}M = \frac{n}{5-n}\frac{GM^2}{R_0}\left(\frac{R_0}{R}\right)^{3/n}. \tag{2.35}$$

Note that $U = 0$ for $n = 0$, since $k_1 = 0$ (cf. LRS1, eq. [2.9]).

3. DYNAMICAL OSCILLATIONS AND STABILITY OF SINGLE STARS

In this section we use the dynamical equations derived in § 2 to study the stability and dynamical oscillations of Riemann-S ellipsoids. We first establish a general criterion for linear stability to small-amplitude dynamical perturbations (§ 3.1). We then study the dynamical oscillations of an ellipsoid, including finite-amplitude self-similar pulsations (§ 3.2) and small-amplitude nonradial oscillations (§ 3.3). Most of the results obtained in this section are well established. The derivations presented here will demonstrate that our formalism can reproduce these results or generalize them to the compressible case.

3.1. *Dynamical Stability Criterion*

Here we show explicitly that the onset of dynamical instability along an equilibrium sequence can be determined from an appropriate energy function defined along that sequence, as we have done in our previous papers (LRS). To do so, we only need to recast the dynamical equations into Hamiltonian form. From the Lagrangian (eq. [2.12]), the canonical momenta associated with the generalized coordinates $\{q_i\} = \{a_1, a_2, a_3, \phi, \psi\}$ are calculated as $P_i = \partial L/\partial q_i$, giving

$$P_{a_i} = \tfrac{1}{5}\kappa_n M\dot{a}_i, \qquad P_\phi = J_s, \qquad P_\psi = \mathscr{C}. \tag{3.1}$$

The Hamiltonian is then

$$H = \sum_i \dot{q}_i P_i - L = \frac{1}{2(\kappa_n M/5)}(P_{a_1}^2 + P_{a_2}^2 + P_{a_3}^2) + E(a_1, a_2, a_3; J_s, \mathscr{C}). \tag{3.2}$$

The energy function E plays the role of an effective potential, and is given by (cf. LRS4, eqs. [2.23] and [2.24], where we make explicit the conserved quantities J_s and $\mathscr{C}$)

$$E(a_1, a_2, a_3; J_s, \mathscr{C}) = \frac{1}{2I_+}(J_s + \mathscr{C})^2 + \frac{1}{2I_-}(J_s - \mathscr{C})^2 + U + W , \tag{3.3}$$

where

$$I_\pm \equiv \tfrac{2}{5}\kappa_n M(a_1 \mp a_2)^2 . \tag{3.4}$$

Hamilton's equations can then be written as

$$\frac{1}{5}\kappa_n M\ddot{a}_i = -\frac{\partial E}{\partial a_i} , \tag{3.5}$$

together with $\dot{J}_s = \dot{\mathscr{C}} = 0$. For linear perturbations we write

$$a_i = a_{i,\,\mathrm{eq}}(1 + \alpha_i) , \tag{3.6}$$

where $|\alpha_i| \ll 1$, and equation (3.5) becomes

$$I_{ii}\ddot{\alpha}_i = -\sum_j \left[\left(\frac{\partial^2 E}{\partial a_i \partial a_j}\right) a_i a_j\right]_{\mathrm{eq}} \alpha_j \qquad \text{(no sum over } i) , \tag{3.7}$$

where $I_{ij} = (\kappa_n/5)Ma_i^2\delta_{ij}$. If we let $\alpha_i \propto e^{i\sigma t}$, equation (3.7) gives

$$\sigma^2 = 0 \Leftrightarrow \det\left(\frac{\partial^2 E}{\partial a_i \partial a_j}\right)_{\mathrm{eq}} = 0 . \tag{3.8}$$

Here a subscript "eq" means evaluating the function for equilibrium configurations. Equation (3.8) is the condition that determines the onset of instability along a sequence of equilibrium configurations (see LRS1, § 2).

3.2. *Homologous Pulsations*

Consider the homologous perturbations described by

$$a_i(t) = \xi(t)a_{i,\,\mathrm{eq}} , \tag{3.9}$$

about a compressible Riemann-S equilibrium configuration. Here $\xi(t)$ is not necessarily close to unity (i.e., we allow for finite-amplitude oscillations). Such oscillations only exist for a compressible ($n \neq 0$) configuration. Our description of the oscillations by equation (3.9) is only approximate (cf. § 3.3), but it is a good approximation for slowly rotating configurations.

Adding $(\kappa_n Ma_1/5) \times$ (eq. [2.19]), $(\kappa_n Ma_2/5) \times$ (eq. [2.20]), and $(\kappa_n Ma_3/5) \times$ (eq. [2.21]), we obtain

$$I_{t,\,\mathrm{eq}}\xi\ddot{\xi} = 2T_s - \frac{|W_{\mathrm{eq}}|}{\xi} + \left(\frac{3k_1 MP_c}{n\rho_c}\right)_{\mathrm{eq}} \xi^{-3/n} , \tag{3.10}$$

where $I_t \equiv I_{11} + I_{22} + I_{33}$, T_s is given by equation (2.6), and we have used equation (2.10) and the fact that $P_c/\rho_c \propto (a_1 a_2 a_3)^{-1/n}$. Since T_s can be written as (LRS4, eqs. [2.23] and [2.24])

$$T_s = \frac{1}{2I_+}(J_s + \mathscr{C})^2 + \frac{1}{2I_-}(J_s - \mathscr{C})^2 , \tag{3.11}$$

and $J_s, \mathscr{C}$ remain constant during a dynamical perturbation, we have

$$T_s = T_{s,\,\mathrm{eq}}\xi^{-2} . \tag{3.12}$$

For the last term in equation (3.10), we use equation (2.30) and the expression

$$\left(\frac{R}{R_0}\right)_{\mathrm{eq}} = \left[f\left(1 - 2\frac{T_s}{|W|}\right)\right]^{-n/(3-n)} \tag{3.13}$$

(LRS1, eq. [4.25]). Equation (3.10) then reduces finally to

$$I_t\ddot{\xi} = |W|(\xi^{-1-3/n} - \xi^{-2}) + 2T_s(\xi^{-3} - \xi^{-1-3/n}) , \tag{3.14}$$

where we have suppressed the subscript "eq." This equation was first derived for an axisymmetric, uniformly rotating polytrope by Tassoul (1970). We see that it applies also to our more general compressible Riemann-S ellipsoids.

Consider now small-amplitude oscillations, with $\xi = 1 + \xi_1$ and $|\xi_1| \ll 1$. Linearization of equation (3.14) yields

$$I_t\ddot{\xi}_1 = |W|\left[(4 - 3\Gamma) - \frac{2T_s}{|W|}(5 - 3\Gamma)\right]\xi_1 . \tag{3.15}$$

We see that stability requires

$$\Gamma > \Gamma_{\rm crit} = \frac{4}{3} - \frac{2T_s/|W|}{3(1-2T_s/|W|)} . \tag{3.16}$$

The corresponding oscillation frequency is given by

$$\sigma^2 = \frac{|W|}{I_t}\left[(3\Gamma-4) - 2\frac{T_s}{|W|}(3\Gamma-5)\right] . \tag{3.17}$$

This is a well-known result (the Ledoux formula), first derived for uniformly and slowly rotating stars (see Tassoul 1978, § 14.2). We see that it can also be applied (approximately) to more general ellipsoidal configurations, even when the rotation rate is large.

For nonrotating stars, equation (3.17) gives the fundamental pulsation mode frequency

$$\sigma_0^2 = \frac{|W|}{I_t}(3\Gamma-4) = \frac{GM}{R_0^3}\frac{1}{q_n}(3\Gamma-4) , \tag{3.18}$$

where $q_n = (1-n/5)\kappa_n$, and κ_n is defined by equation (2.7). The values of κ_n for different n are given in Table 1 of LRS1. In Table 1 here, we compare the predictions of equation (3.18) with the exact results obtained by integrating numerically the radial pulsation equation for polytropes with $\Gamma = \Gamma_1$ (Cox 1980, chap. 8). We see that equation (3.18) predicts the exact results remarkably well. The discrepancy remains less than $\sim 3\%$ for all values of n. For $n = 3$ and in the limit as $n \to 0$, equation (3.18) yields the exact results. This is not surprising, since, in these limits, small radial pulsations in the fundamental mode are indeed homologous. The excellent agreement for all n gives us confidence that our treatment of small dynamical perturbations is always a very good approximation.

We can also consider the stability to finite-amplitude oscillations (Tassoul 1970). Integrating equation (3.14) once, we obtain

$$\tfrac{1}{2}I_t\dot{\xi}^2 + |W|\Psi(\xi) = \text{constant} , \tag{3.19}$$

where

$$\Psi(\xi) = \frac{T_s/|W| - \xi}{\xi^2} + \frac{1-2T_s/|W|}{3(\Gamma-1)\xi^{3(\Gamma-1)}} . \tag{3.20}$$

From equation (3.19) we see that $\Psi(\xi)$ acts like an effective potential for the oscillation. It is easy to see that $\xi = 1$ is a local minimum of $\Psi(\xi)$ only when condition (3.16) is satisfied. But even then it is not necessarily a global minimum. Consider the behavior of $\Psi(\xi)$ for $\xi \gg 1$,

$$\Psi(\xi) \simeq \frac{1}{\xi}\left[-1 + \frac{1-2T_s/|W|}{3(\Gamma-1)\xi^{3\Gamma-4}}\right] . \tag{3.21}$$

We see that when $\Gamma < 4/3$, $\Psi(\xi)$ has a global minimum at $\xi = \infty$. Thus for $\Gamma_{\rm crit} < \Gamma < 4/3$, the star is only metastable (Tassoul 1970). The condition for stability to finite-amplitude dynamical perturbations is $\Gamma > 4/3$, independent of rotation.

3.3. *General Oscillations of a Maclaurin Spheroid*

We now consider the general linear oscillations

$$a_i(t) = a_{i,\rm eq}(1+\alpha_i) , \tag{3.22}$$

with $|\alpha_i| \ll 1$. For simplicity we assume $a_{1,\rm eq} = a_{2,\rm eq}$, i.e., the equilibrium configuration is a compressible Maclaurin spheroid.

We must linearize equations (2.19)–(2.23) to obtain the dynamical equations for α_i. In the derivation, one must be careful to note that a Maclaurin spheroid need not be assigned the angular velocity of the frame in which it is at rest, i.e., the value of $\Omega_{\rm eq}$ and $\Lambda_{\rm eq}$ must be determined, like the frequency σ, from the analysis (Rossner 1967). Here we will use equation (3.7) directly. For a Maclaurin

TABLE 1

RADIAL PULSATIONS OF POLYTROPES[a]

n	$\hat{\sigma}_0^2$	q_n^{-1}
0.....	1	1
0.5.....	1.355	1.364
1.0.....	1.877	1.913
1.5.....	2.706	2.793
2.0.....	4.137	4.305
2.5.....	6.909	7.155
3.0.....	13.27	13.27

[a] Here $\hat{\sigma}_0^2 \equiv \sigma_0^2/[(3\Gamma-4)GM/R_0^3]$ and $\Gamma = \Gamma_1 = 1 + 1/n$.

spheroid we have $J_s = -\mathscr{C}$ (cf. eqs. [2.17] and [2.18] for $a_1 = a_2$), and the kinetic energy term is simply

$$T_s = \frac{J_s^2}{(\kappa_n/5)M(a_1 + a_2)^2} . \tag{3.23}$$

Setting the first derivatives of E equal to zero, we obtain the equilibrium conditions

$$T_s = -\Sigma(a_1^2 A_1 - a_3^2 A_3) , \qquad \frac{1}{n} U = -\Sigma a_3^2 A_3 , \tag{3.24}$$

where we have defined

$$\Sigma \equiv -\frac{3GM^2}{2(5-n)R^3} , \tag{3.25}$$

so that $W = \Sigma \mathscr{I}$. For convenience we also define

$$\mathscr{E}_{ij} \equiv \left(a_i a_j \frac{\partial^2 E}{\partial a_i \partial a_j} \right)_{\rm eq} . \tag{3.26}$$

After some algebra we obtain the following expressions:

$$\begin{aligned}
\mathscr{E}_{11} &= \mathscr{E}_{22} = \frac{1}{n}\left(1 + \frac{1}{n}\right)U - a_1^2\Sigma(3B_{11} - 2A_1) + \frac{3}{2}T_s , \\
\mathscr{E}_{33} &= \frac{1}{n}\left(1 + \frac{1}{n}\right)U + 2a_3^2\Sigma B_{13} , \\
\mathscr{E}_{12} &= \frac{1}{n^2} U - a_1^2\Sigma(B_{11} - A_1) + \frac{3}{2} T_s , \\
\mathscr{E}_{13} &= \mathscr{E}_{23} = \frac{1}{n^2} U - a_1^2\Sigma(B_{13} - A_1) ,
\end{aligned} \tag{3.27}$$

where the B_{ij} are defined as in Ch69 (chap. 3) and the right-hand sides are evaluated for the equilibrium configuration (the subscript "eq" has been dropped). Let $\alpha_i \propto e^{i\sigma t}$. The linearized equations for small oscillations then give

$$\begin{pmatrix} \mathscr{E}_{11} - I_{11}\sigma^2 & \mathscr{E}_{12} & \mathscr{E}_{13} \\ \mathscr{E}_{12} & \mathscr{E}_{11} - I_{11}\sigma^2 & \mathscr{E}_{13} \\ \mathscr{E}_{13} & \mathscr{E}_{13} & \mathscr{E}_{33} - I_{33}\sigma^2 \end{pmatrix} \begin{pmatrix} \alpha_1 \\ \alpha_2 \\ \alpha_3 \end{pmatrix} = 0 . \tag{3.28}$$

We now determine the eigenfrequencies and eigenmodes by solving the linear system (3.28). One of the eigenvalues can be obtained from

$$I_{11}\sigma^2 = \mathscr{E}_{11} - \mathscr{E}_{12} = \frac{1}{n} U - a_1^2\Sigma(2B_{11} - A_1) . \tag{3.29}$$

Using the equilibrium conditions (3.24), we obtain

$$\bar{\sigma}^2 = \frac{4}{q_n} B_{11} - \bar{\Omega}^2 , \tag{3.30}$$

where $\bar{\sigma} \equiv \sigma/(\pi G\bar{\rho})^{1/2}$, $\bar{\Omega} \equiv \Omega/(\pi G\bar{\rho})^{1/2}$, and $\bar{\rho} = 3M/(4\pi R^3)$ is the mean density. The corresponding eigenmode has the form

$$\begin{pmatrix} \alpha_1 \\ \alpha_2 \\ \alpha_3 \end{pmatrix} \propto \begin{pmatrix} 1 \\ -1 \\ 0 \end{pmatrix} . \tag{3.31}$$

This mode is the compressible generalization of the *toroidal mode* found in Ch69 (or bar mode). In a reference frame corotating with the unperturbed star, fluid elements oscillate at a frequency σ_0 given by

$$\bar{\sigma}_0 = \bar{\Omega} \pm \bar{\sigma} = \bar{\Omega} \pm \left(\frac{4}{q_n} B_{11} - \bar{\Omega}^2 \right)^{1/2} . \tag{3.32}$$

This expression agrees with the result (5.50) of Ch69 for $n = 0$. We see that the onset of dynamical instability is given by

$$\bar{\Omega}^2 = \bar{\Omega}_{\rm dyn}^2 \equiv \frac{4}{q_n} B_{11} . \tag{3.33}$$

The toroidal mode is neutrally stable as seen in the corotating frame ($\sigma_0 = 0$) when

$$\bar{\Omega}^2 = \bar{\Omega}_{\rm bif}^2 \equiv \frac{2}{q_n} B_{11} , \tag{3.34}$$

corresponding to the point where the Jacobi sequence bifurcates from the Maclaurin sequence (Ch69; LRS1).

The eigenfrequencies for the two other modes are determined from

$$(\mathscr{E}_{11} + \mathscr{E}_{12} - I_{11}\sigma^2)(\mathscr{E}_{33} - I_{33}\sigma^2) = 2\mathscr{E}_{13}^2 , \tag{3.35}$$

and the corresponding eigenmodes have the form

$$\begin{pmatrix} \alpha_1 \\ \alpha_2 \\ \alpha_3 \end{pmatrix} \propto \begin{pmatrix} 1 \\ 1 \\ \alpha_3/\alpha_1 \end{pmatrix} . \tag{3.36}$$

For these two modes the linearized equations reduce to

$$\begin{pmatrix} \mathscr{E}_{11} + \mathscr{E}_{12} - I_{11}\sigma^2 & \mathscr{E}_{13} \\ 2\mathscr{E}_{13} & \mathscr{E}_{33} - I_{33}\sigma^2 \end{pmatrix} \begin{pmatrix} \alpha_1 \\ \alpha_3 \end{pmatrix} = 0 . \tag{3.37}$$

For $n \neq 0$ these two modes are somewhat similar to the homologous pulsations discussed in § 3.2. They are also the compressible generalization of the *zonal modes* discussed by Ch69 and Tassoul (1978). Since $\alpha_3 \neq \alpha_1$, the deformation is not homologous and the results obtained in § 3.2 are slightly modified. In particular, setting $\sigma = 0$ in equation (3.37), we obtain the critical Γ for dynamical stability,

$$\Gamma_{\rm crit} = \frac{4}{3} - \frac{2T_s}{3|W|}\left[1 - \left(2 + \frac{A_3}{3B_{13} - 2A_3}\right)\frac{T_s}{|W|}\right]^{-1} . \tag{3.38}$$

This stability condition is slightly *more restrictive* than equation (3.16), since a more general trial function has been used here. With some algebra it can be shown that expression (3.38) agrees with the result derived in LRS1 (eq. [6.3]).

The expressions for the eigenfrequencies are quite complicated for general n. For $n = 0$ the result is simpler. Subtracting the two equations in (3.37) from each other, taking the $n \to 0$ limit, and using the equilibrium conditions (3.24), we obtain

$$\begin{pmatrix} 2 & 1 \\ I_{11}\sigma^2 + (4a_1^2 B_{11} - 2a_3^2 B_{13})\Sigma & (3a_3^2 B_{13} - 2a_3^2 A_3)\Sigma - I_{33}\sigma^2 \end{pmatrix} \begin{pmatrix} \alpha_1 \\ \alpha_3 \end{pmatrix} = 0 \qquad (n = 0) . \tag{3.39}$$

The eigenfrequency is given by

$$\bar{\sigma}^2 = \left[4B_{11} + \frac{a_3^2}{a_1^2}(6B_{33} - 4B_{13})\right]\left(\frac{1}{2} + \frac{a_3^2}{a_1^2}\right)^{-1} \qquad (n = 0) . \tag{3.40}$$

This is identical to the result given by Ch69 (eq. [5.63]). The corresponding eigenmode is

$$\begin{pmatrix} \alpha_1 \\ \alpha_2 \\ \alpha_3 \end{pmatrix} \propto \begin{pmatrix} 1 \\ 1 \\ -2 \end{pmatrix} \qquad (n = 0) . \tag{3.41}$$

For a nonrotating (spherical) star with $n = 0$, the toroidal mode (3.31) is simply the $l = 2$, $m = \pm 2$ Kelvin mode, while the mode (3.41) describes axisymmetric pulsations with $l = 2$, $m = 0$. With $B_{ij} = 4/15$ for a sphere, equations (3.30) and (3.40) both give $\bar{\sigma}^2 = 16/15$, an exact result for the frequency of the Kelvin mode.

Note that the "transverse-shear modes" discussed by Ch69 (§ 33) cannot be incorporated in our treatment, since they involve perturbations of the rotation axis.

4. DISSIPATIVE EFFECTS FOR A SINGLE STAR

We now incorporate dissipative forces into the dynamical equations derived in § 2. In general, dissipation modifies the Euler-Lagrange equations according to

$$\frac{d}{dt}\frac{\partial L}{\partial \dot{q}_i} = \frac{\partial L}{\partial q_i} + \mathscr{F}_{q_i} , \tag{4.1}$$

where $\mathscr{F}_{q_i}$ is the generalized dissipative force associated with the coordinate q_i. The generalized dissipative forces are defined so that the dissipation rate $\mathscr{W}$ (Rayleigh's dissipation function; cf. Goldstein 1980) can be written

$$\mathscr{W} = \mathscr{F}_{q_i}\dot{q}_i . \tag{4.2}$$

Therefore, to calculate $\mathscr{F}_{q_i}$, we need to evaluate $\mathscr{W}$ and express it in terms of q_i and $\dot{q}_i$.

4.1. *Viscous Dissipation*

The dissipation rate due to shear viscosity is given by (cf. Landau & Lifshitz 1987)

$$\mathcal{W} = -\int \sigma_{ij} u_{i,j} d^3x \,, \tag{4.3}$$

where u_i is the fluid velocity and σ_{ij} is the viscous stress tensor,

$$\sigma_{ij} = \eta(u_{i,j} + u_{j,i} - \tfrac{2}{3}\delta_{ij}\nabla \cdot \boldsymbol{u}) \,, \tag{4.4}$$

We denote by $\eta = \rho\nu$ the dynamical shear viscosity, where ν is the kinematic shear viscosity. The bulk viscosity will be neglected. From equations (2.2)–(2.4) we have

$$\begin{aligned} u_{1,1} &= \frac{\dot{a}_1}{a_1} \,, \qquad u_{2,2} = \frac{\dot{a}_2}{a_2} \,, \qquad u_{3,3} = \frac{\dot{a}_3}{a_3} \,, \\ u_{1,2} &= \frac{a_1}{a_2}\Lambda - \Omega \,, \\ u_{2,1} &= -\frac{a_2}{a_1}\Lambda + \Omega \,, \\ u_{i,j} &= 0 \qquad \text{otherwise} \,. \end{aligned} \tag{4.5}$$

Thus the viscous dissipation rate is given by

$$\mathcal{W} = -\frac{4}{3}\bar{\nu}M\left[\left(\frac{\dot{a}_1}{a_1}\right)^2 + \left(\frac{\dot{a}_2}{a_2}\right)^2 + \left(\frac{\dot{a}_3}{a_3}\right)^2 - \left(\frac{\dot{a}_1}{a_1}\right)\left(\frac{\dot{a}_2}{a_2}\right) - \left(\frac{\dot{a}_1}{a_1}\right)\left(\frac{\dot{a}_3}{a_3}\right) - \left(\frac{\dot{a}_2}{a_2}\right)\left(\frac{\dot{a}_3}{a_3}\right)\right] - \bar{\nu}M\Lambda^2\left(\frac{a_1^2 - a_2^2}{a_1 a_2}\right)^2 \,, \tag{4.6}$$

where $\bar{\nu}$ is the mass-averaged shear viscosity

$$\bar{\nu} = \frac{1}{M}\int \nu \, dm \,. \tag{4.7}$$

Since $\mathcal{W}$ in equation (4.6) is quadratic in $\dot{q}_i$, from equation (4.2), the dissipative forces are given by

$$\mathcal{F}_{q_i} = \frac{1}{2}\frac{\partial \mathcal{W}}{\partial \dot{q}_i} \,. \tag{4.8}$$

Thus we have

$$\begin{aligned} \mathcal{F}_{a_1} &= -\frac{2}{3}\bar{\nu}M\left(2\frac{\dot{a}_1}{a_1} - \frac{\dot{a}_2}{a_2} - \frac{\dot{a}_3}{a_3}\right)\frac{1}{a_1} \,, \\ \mathcal{F}_{a_2} &= -\frac{2}{3}\bar{\nu}M\left(2\frac{\dot{a}_2}{a_2} - \frac{\dot{a}_1}{a_1} - \frac{\dot{a}_3}{a_3}\right)\frac{1}{a_2} \,, \\ \mathcal{F}_{a_3} &= -\frac{2}{3}\bar{\nu}M\left(2\frac{\dot{a}_3}{a_3} - \frac{\dot{a}_1}{a_1} - \frac{\dot{a}_2}{a_2}\right)\frac{1}{a_3} \,, \\ \mathcal{F}_{\phi} &= 0 \,, \\ \mathcal{F}_{\psi} &= -\bar{\nu}M\Lambda\left(\frac{a_1^2 - a_2^2}{a_1 a_2}\right)^2 \,. \end{aligned} \tag{4.9}$$

The statement $\mathcal{F}_\phi = 0$ simply indicates that viscous forces conserve angular momentum ($dJ_s/dt = \mathcal{F}_\phi = 0$), while they do not conserve fluid circulation, since $d\mathcal{C}/dt = \mathcal{F}_\psi \neq 0$.

In the presence of viscous dissipation, the dynamical equations (2.19)–(2.23) become

$$\ddot{a}_1 = \{\cdots\} - \frac{10}{3\kappa_n}\bar{\nu}\left(\frac{2\dot{a}_1}{a_1} - \frac{\dot{a}_2}{a_2} - \frac{\dot{a}_3}{a_3}\right)\frac{1}{a_1} \,, \tag{4.10}$$

$$\ddot{a}_2 = \{\cdots\} - \frac{10}{3\kappa_n}\bar{\nu}\left(\frac{2\dot{a}_2}{a_2} - \frac{\dot{a}_1}{a_1} - \frac{\dot{a}_3}{a_3}\right)\frac{1}{a_2} \,, \tag{4.11}$$

$$\ddot{a}_3 = \{\cdots\} - \frac{10}{3\kappa_n}\bar{\nu}\left(\frac{2\dot{a}_3}{a_3} - \frac{\dot{a}_1}{a_1} - \frac{\dot{a}_2}{a_2}\right)\frac{1}{a_3} \,, \tag{4.12}$$

$$\frac{d}{dt}(a_1\Omega - a_2\Lambda) = \{\cdots\} - \frac{5}{\kappa_n}\bar{\nu}\frac{a_1^2 - a_2^2}{a_1^2 a_2}\Lambda\,, \tag{4.13}$$

$$\frac{d}{dt}(-a_2\Omega + a_1\Lambda) = \{\cdots\} - \frac{5}{\kappa_n}\bar{\nu}\frac{a_1^2 - a_2^2}{a_1 a_2^2}\Lambda\,, \tag{4.14}$$

where $\{\cdots\}$ denotes the terms that already exist in equations (2.19)–(2.23) (This notation will be used throughout the paper). For the pressure term, expression (2.30) still applies here, but expression (2.34) must be modified as

$$\frac{2P_c}{\rho_c} = \left(\sum_i \frac{1}{a_i^2}\right)^{-1}\left[\{\cdots\} + 10\bar{\nu}\sum_i \frac{\dot{a}_i}{a_i^3}\right] \qquad (n = 0)\,. \tag{4.15}$$

Equations (2.24) and (2.25) become

$$\begin{aligned}\dot{\Omega} &= \left(\frac{a_2}{a_1} - \frac{a_1}{a_2}\right)^{-1}\left[\{\cdots\} + \frac{10}{\kappa_n}\bar{\nu}\frac{a_1^2 - a_2^2}{a_1^2 a_2^2}\Lambda\right],\\ \dot{\Lambda} &= \left(\frac{a_2}{a_1} - \frac{a_1}{a_2}\right)^{-1}\left[\{\cdots\} + \frac{5}{\kappa_n}\bar{\nu}\frac{a_1^2 - a_2^2}{a_1 a_2}\left(\frac{1}{a_1^2} + \frac{1}{a_2^2}\right)\Lambda\right].\end{aligned} \tag{4.16}$$

Recall that the energy dissipation rate is simply $\dot{\mathscr{E}} = \mathscr{W}$. For a quasi-static ellipsoid, this rate reduces to equation (6.4) in LRS4.

4.2. *Gravitational Radiation Reaction*

In the weak-field, slow-motion regime of general relativity, the emission of gravitational waves induces a back-reaction scalar potential $\Phi_{\rm react}$ which can be written as (Misner, Thorne, & Wheeler 1973)

$$\Phi_{\rm react} = \frac{G}{5c^5} I_{ij}^{(5)} x_i x_j\,, \tag{4.17}$$

where the superscript (5) indicates the fifth time derivative and c is the speed of light. Here we choose x_i ($i = 1, 2, 3$) to be the Cartesian coordinates of a fluid element in the instantaneous corotating frame (the body frame, with basis vectors along the principal axes). Then $I_{ij}^{(5)}$ is the fifth time derivative of the reduced quadrupole moment tensor of the system in the inertial frame *projected onto the body frame*. Expressions for $I_{ij}^{(5)}$ are given in the Appendix. The radiation reaction force per unit mass on the fluid is $-\nabla\Phi_{\rm react}$. The energy dissipation rate is thus given by

$$\mathscr{W} = -\int \boldsymbol{u}\cdot\nabla\Phi_{\rm react}\, dm\,. \tag{4.18}$$

Using equations (2.2)–(2.4), we get

$$\mathscr{W} = -\left(\frac{1}{5}\kappa_n M\right)\frac{2G}{5c^5}\left[I_{11}^{(5)}\dot{a}_1 a_1 + I_{22}^{(5)}\dot{a}_2 a_2 + I_{33}^{(5)}\dot{a}_3 a_3 + I_{12}^{(5)}\Omega(a_1^2 - a_2^2)\right], \tag{4.19}$$

where we have used

$$\int x_i x_j\, dm \equiv I_{ij} = \tfrac{1}{5}\kappa_n M a_i^2\delta_{ij}\,. \tag{4.20}$$

Since $\mathscr{W}$ here is linear in q_i, the dissipative forces due to gravitational radiation are given by (compare eq. [4.8])

$$\mathscr{F}_{q_i} = \frac{\partial\mathscr{W}}{\partial\dot{q}_i}\,. \tag{4.21}$$

From equations (4.19) and (4.21) we obtain

$$\begin{aligned}\mathscr{F}_{a_1} &= -\left(\frac{1}{5}\kappa_n M\right)\frac{2G}{5c^5} I_{11}^{(5)} a_1\,,\\ \mathscr{F}_{a_2} &= -\left(\frac{1}{5}\kappa_n M\right)\frac{2G}{5c^5} I_{22}^{(5)} a_2\,,\\ \mathscr{F}_{a_3} &= -\left(\frac{1}{5}\kappa_n M\right)\frac{2G}{5c^5} I_{33}^{(5)} a_3\,,\\ \mathscr{F}_{\phi} &= -\left(\frac{1}{5}\kappa_n M\right)\frac{2G}{5c^5} I_{12}^{(5)}(a_1^2 - a_2^2)\,,\\ \mathscr{F}_{\psi} &= 0\,.\end{aligned} \tag{4.22}$$

Since $\mathscr{F}_\psi = 0$, we see that *the gravitational radiation reaction conserves the fluid circulation*, i.e., $d\mathscr{C}/dt = \mathscr{F}_\psi = 0$. But since $\mathscr{F}_\phi \neq 0$, the total angular momentum is not conserved in general. Indeed, gravitational waves can carry away angular momentum as well as energy when the system is not axisymmetric.

Including the gravitational radiation reaction, the dynamical equations (2.19)–(2.23) become

$$\ddot{a}_1 = \{\cdots\} - \frac{2G}{5c^5} I^{(5)}_{11} a_1 , \tag{4.23}$$

$$\ddot{a}_2 = \{\cdots\} - \frac{2G}{5c^5} I^{(5)}_{22} a_2 , \tag{4.24}$$

$$\ddot{a}_3 = \{\cdots\} - \frac{2G}{5c^5} I^{(5)}_{33} a_3 , \tag{4.25}$$

$$\frac{d}{dt}(a_1\Omega - a_2\Lambda) = \{\cdots\} - \frac{2G}{5c^5} I^{(5)}_{12} a_1 , \tag{4.26}$$

$$\frac{d}{dt}(-a_2\Omega + a_1\Lambda) = \{\cdots\} - \frac{2G}{5c^5} I^{(5)}_{12} a_2 . \tag{4.27}$$

Since $I^{(5)}_{11} + I^{(5)}_{22} + I^{(5)}_{33} = 0$, it can be shown easily that the expression for $2P_c/\rho_c$ is not affected by the presence of the gravitational radiation reaction, i.e., equations (2.30) and (2.34) still apply. Equations (2.24) and (2.25) are modified as

$$\begin{aligned} \dot{\Omega} &= \left(\frac{a_2}{a_1} - \frac{a_1}{a_2}\right)^{-1}\left[\{\cdots\} + \frac{2G}{5c^5} I^{(5)}_{12}\left(\frac{a_1}{a_2} + \frac{a_2}{a_1}\right)\right], \\ \dot{\Lambda} &= \left(\frac{a_2}{a_1} - \frac{a_1}{a_2}\right)^{-1}\left[\{\cdots\} + \frac{4G}{5c^5} I^{(5)}_{12}\right]. \end{aligned} \tag{4.28}$$

As before, the energy loss rate is simply $\dot{\mathscr{E}} = \mathscr{W}$.

4.3. *Secular Evolution of a Compressible Ellipsoid*

The secular evolution of incompressible ellipsoids in the presence of dissipation has been studied previously. Using a linear perturbation analysis, Roberts & Stewartson (1963) and Chandrasekhar (1970) demonstrated that the presence of either viscosity or the gravitational radiation reaction induces a secular instability of incompressible spheroids on the Maclaurin sequence beyond the point where the Jacobi and Dedekind sequences branch off. Press & Teukolsky (1973) have studied the viscous evolution of a secularly unstable incompressible Maclaurin spheroid, and Miller (1974) has integrated the Riemann-Lebovitz equations for incompressible ellipsoids including the effects of gravitational radiation reaction.

Our dynamical equations represent a generalization to compressible ellipsoids of the equations considered by Press & Teukolsky (1973) and Miller (1974). We have integrated our equations for a variety of compressible ellipsoidal configurations, and have found results similar to those obtained in these previous studies for incompressible ellipsoids.

The secular evolutionary paths of the ellipsoids can be understood clearly in terms of the energetics and conservation principles: dissipative forces always drive a system toward a state with lower energy, along quasi-equilibrium paths that hold conserved quantities fixed. Consider first the evolution of an ellipsoid under the gravitational radiation reaction. Since the radiation reaction forces conserve the fluid circulation (cf. eq. [4.22]), such an evolution is always along a constant-$\mathscr{C}$ sequence. In Figure 1 we show the variation of the total energy along various constant-$\mathscr{C}$ sequences (with $n = 1$) as a function of the axis ratio a_2/a_1. The curves were obtained numerically by solving the Riemann-S equilibrium equations (LRS1, § 5). Note that a given Maclaurin spheroid corresponds to a unique value of $\mathscr{C}$, but two different constant-$\mathscr{C}$ sequences branch off: one sequence is *Jacobi-like*, with $|\Omega| > |\Lambda|$, and the other is *Dedekind-like*, with $|\Lambda| > |\Omega|$.[4] For given values of $\mathscr{C}$ and a_2/a_1, the Jacobi-like configuration has higher energy than the Dedekind-like configuration. Also shown in Figure 1 is the Dedekind sequence (of configurations with $\Lambda/\Omega = \infty$) and the Jacobi sequence ($\Lambda/\Omega = 0$), which bifurcate from the Maclaurin sequence ($a_2/a_1 = 1$) at the point where the ratio $T_s/|W| = 0.1375$ (in our approximation this value is independent of n; see LRS1, § 4). Note that the Dedekind sequence and the Jacobi sequence are adjoints of each other and therefore have the same energy for given a_2/a_1 (see LRS1, § 5.1).

We see from Figure 1 that there exists a critical value of $|\mathscr{C}| = |\mathscr{C}_{\rm sec}|$, equal to the absolute value of the circulation of a Maclaurin spheroid at the bifurcation point, below which a constant-$\mathscr{C}$ sequence has a Maclaurin spheroid as its minimum-energy state and above which its minimum-energy state is a Dedekind ellipsoid. Therefore, an initial configuration with $|\mathscr{C}| < |\mathscr{C}_{\rm sec}|$ will evolve to become a Maclaurin spheroid under the gravitational radiation reaction. For an initial configuration with $|\mathscr{C}| > |\mathscr{C}_{\rm sec}|$, the final state is a Dedekind ellipsoid. In the latter case, however, if $|\Omega| > |\Lambda|$, the system will first evolve to a Maclaurin spheroid; only when some additional perturbation (e.g., viscosity) triggers the secularly unstable bar mode of the Maclaurin spheroid does the system evolve past the Maclaurin sequence, toward a final Dedekind ellipsoid. Note that the evolutionary timescale of the Dedekind-like phase is much longer than that of the Jacobi-like phase, as a result of the steep power-law dependence of the energy dissipation rate on Ω (cf. Lai & Shapiro 1994a).

[4] Such a characterization of the two branches (as used by Detweiler & Lindblom 1977) is not exact. When the deformation is very large, e.g., $a_2/a_1 \leq 0.1$, we find that both configurations have $|\Omega| > |\Lambda|$. However, except for such highly deformed configurations, the two branches do have $|\Omega| > |\Lambda|$ or $|\Lambda| > |\Omega|$. More appropriate is using $|\zeta/\Omega| < 2$ to define Jacobian-like and $|\zeta/\Omega| > 2$ to define Dedekind-like, where ζ is the vorticity in the corotating frame.

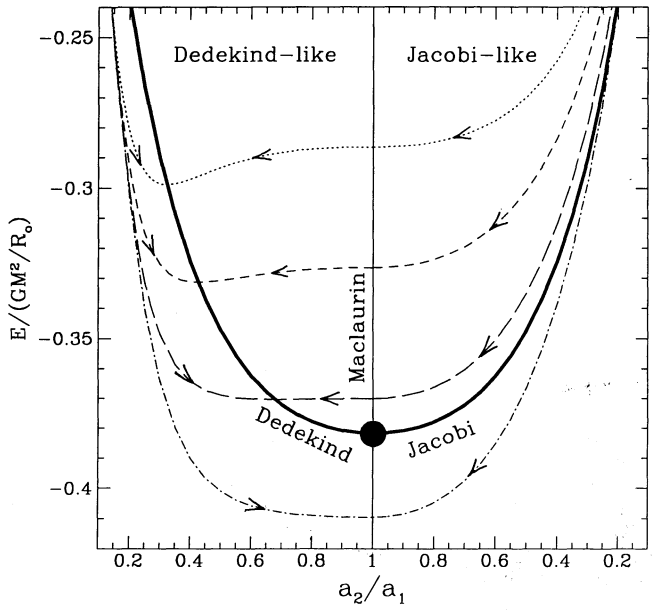

FIG. 1

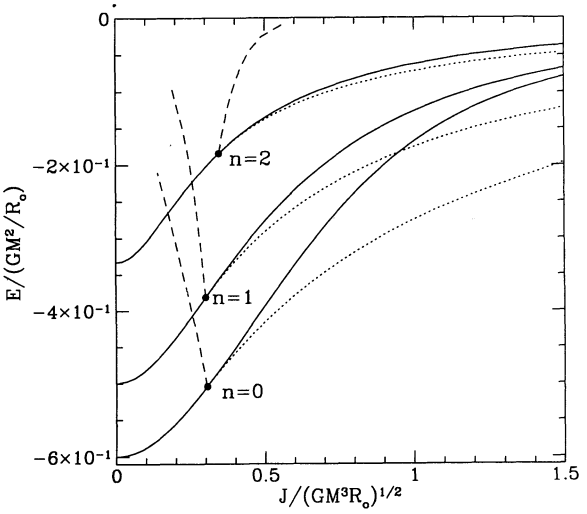

FIG. 2

FIG. 1.—Secular evolution tracks of a Riemann-S ellipsoid with $n = 1$ driven by gravitational radiation reaction. The energy of an ellipsoid as a function of the axis ratio a_2/a_1 is shown along various equilibrium sequences. Dedekind-like sequences ($|\Lambda| > |\Omega|$) are shown on the left, Jacobi-like ($|\Omega| > |\Lambda|$) on the right. The thick solid line corresponds to the Dedekind and Jacobi sequences, while the other lines correspond to constant-$\mathscr{C}$ sequences: $\bar{\mathscr{C}} = \mathscr{C}/(GM^3R_0)^{1/2} = -0.48$ (*dotted line*), $\bar{\mathscr{C}} = -0.4$ (*dashed line*), $\bar{\mathscr{C}} = -0.32$ (*long-dashed line*), and $\bar{\mathscr{C}} = -0.25$ (*dot-dash line*). The solid round dot marks the point of bifurcation. This figure can also be applied to pure viscous evolution, in which case the curves for Jacobi-like sequences and Dedekind-like sequences are switched, and $\mathscr{C}$ is replaced by $J = -\mathscr{C}$ = constant.

FIG. 2.—Energy as a function of angular momentum for Maclaurin (*solid lines*), Jacobi (*dotted lines*), and Dedekind (*dashed lines*) equilibrium sequences, for $n = 0$, 1, 2.

The evolution of ellipsoids under pure viscous dissipation can be understood similarly. As viscosity conserves J (see eq. [4.9]) while dissipating energy, the evolution is along a constant-J sequence. From Dedekind's theorem (Ch69, chap 3; LRS1, § 5.1), we know that the energy curves of constant-J sequences are identical to those of constant-$\mathscr{C}$ curves, e.g., a Jacobi-like constant-J sequence is adjoint to a Dedekind-like constant-$\mathscr{C}$ sequence with $\mathscr{C} = -J$. Therefore, Figure 1 can be used again here, but after switching the curves for Jacobi-like sequences and Dedekind-like sequences. We see that the final state is either a secularly stable Maclaurin spheroid (when $J < J_{\rm sec}$) or a Jacobi ellipsoid (when $J > J_{\rm sec}$).

The difference in the evolution for different polytropic indices n is illustrated in Figure 2, where we show the E versus J curves of Maclaurin, Jacobi, and Dedekind sequences for various n. In the presence of viscosity, and ellipsoid evolves vertically donward in this diagram, and the evolution terminates at a corresponding Maclaurin spheroid or Jacobi ellipsoid. We see that for small $n \lesssim 1.5$ a Dedekind ellipsoid evolves to a secularly stable Maclaurin spheroid; but for large $n \gtrsim 1.5$ a Dedekind ellipsoid first evolves toward a secularly unstable Maclaurin spheroid, and finally to a Jacobi ellipsoid. This qualitative difference is easy to understand: a highly compressible configuration can expand appreciably when deformed, giving a larger angular momentum (this can also be seen using the scaling relation for Riemann-S ellipsoids; cf. eq. [3.27] in LRS1).

Similarly, Figure 2 can be used to understand the evolution driven by the gravitational radiation reaction. In this case, the horizontal axis represents $-\mathscr{C}$, and curves for Jacobi and Dedekind sequences are switched. Thus we see that for small n a Jacobi ellipsoid evolves to a Maclaurin spheroid, while for large n its final state is a Dedekind ellipsoid. One of the outstanding problems of three-dimensional hydrodynamics with gravitational radiation is to verify this behavior using the exact hydrodynamic equations. The result has important consequences for the fate of nonaxisymmetric, rapidly rotating neutron stars, and for coalescing binary neutron stars (see Rasio & Shapiro 1994, § 4.1).

Lindblom & Detweiler (1977) have considered the combined effects of gravitational radiation reaction and viscosity on the stability of incompressible Maclaurin spheroids. Based on a linear analysis, they showed that when operating together, the two effects tend to cancel each other. Evolutionary tracks of general ellipsoids for various ratios of the viscous timescale and the radiation-reaction timescale have been obtained by Detweiler & Lindblom (1977). Using our dynamical equations, we can now extend this study to compressible ellipsoids (Lai & Shapiro 1994a).

4.4. *Secular Instability Growth Time*

We have derived the secular instability growth time for a compressible Maclaurin spheroid, both with viscosity and the gravitational radiation reaction (Lai & Shapiro 1994a). The viscous instability growth time $\tau_{\rm vis}$ is given by

$$\tau_{\rm vis}^{-1} = \frac{5\bar{\nu}}{\kappa_n a_1^2}\left(\frac{\Omega - \sigma}{\sigma}\right), \tag{4.29}$$

while the growth time τ_{GR} of the instability driven by the gravitational radiation reaction is given by

$$\tau_{GR}^{-1} = \frac{2G\kappa_n M a_1^2}{25c^5} \frac{(\Omega - \sigma)^5}{\sigma} . \tag{4.30}$$

Here σ is the eigenfrequency of the toroidal mode in the absence of dissipation, given by equation (3.30), and κ_n is defined by equation (2.7). In the $n = 0$ limit, these results agree with those given by Ch69 (§ 37) for the viscous instability and by Chandrasekhar (1970) for the gravitational radiation reaction.

A more complete discussion of the instabilities and secular evolution of rotating stars will be presented elsewhere (Lai & Shapiro 1994a), together with an application to the emission of gravitational waves during core collapse.

5. DYNAMICAL EQUATIONS FOR BINARIES: ROCHE-RIEMANN SYSTEMS

Having studied in detail the evolution of single stars modeled as compressible Riemann-S ellipsoids, we now turn to binary systems. We will derive the general dynamical equations for a bound or unbound system containing a compressible Riemann-S ellipsoid and a *point mass* (a Roche-Riemann binary system). For parabolic orbits, Nduka (1971) first derived the dynamical Riemann-Lebovitz equations in the incompressible limit.[5] In addition to providing a generalization to compressible ellipsoids, our equations also determine the orbital dynamics self-consistently, thus allowing for general binary orbits. Equilibrium Roche-Riemann binaries in circular orbit have been studied in LRS1 (§ 8; see also Aizenman 1968).

In addition to the coordinates $\{a_i, \phi, \psi\}$ used in § 2 to describe the structure of a single ellipsoid, we need to introduce new variables to specify the orbital motion and the relative orientation of the ellipsoid. For simplicity we consider only orbits *in the equatorial plane* of the ellipsoid (i.e., with the orbital angular momentum and the spin of the ellipsoid aligned along $\boldsymbol{e}_3$). Two new coordinates are then needed to describe the orbit: a radial coordinate r which measures the separation between the center of mass of the ellipsoid and the point mass, and an angular coordinate θ which we take to be the true anomaly of the point mass. We also define a *misalignment angle* $\alpha = \theta - \phi$ between the axis a_1 of the ellipsoid and the line joining the centers of the two bodies (see Fig. 3). The point mass is called M', and, following Ch69 and LRS, we denote the mass ratio by $p = M/M'$.

The Lagrangian of the system is simply the sum of the single ellipsoid contribution, L_s, given by equations (2.8)–(2.12), and an orbital contribution, L_{orb},

$$L = L_s + L_{orb} , \tag{5.1}$$

where

$$L_{orb} = \tfrac{1}{2}\mu\dot{r}^2 + \tfrac{1}{2}\mu r^2\dot{\theta}^2 - W_i . \tag{5.2}$$

The first two terms in equation (5.2) give the orbital kinetic energy, and the last term W_i is the interaction energy between M and M', given by

$$W_i = -GM' \int d^3x \frac{\rho(\boldsymbol{x})}{|\boldsymbol{r} - \boldsymbol{x}|} , \tag{5.3}$$

[5] Misprints and errors in the original paper by Nduka have been pointed out by Luminet & Carter (1986, p. 224) and by Kosovichev & Novikov (1992).

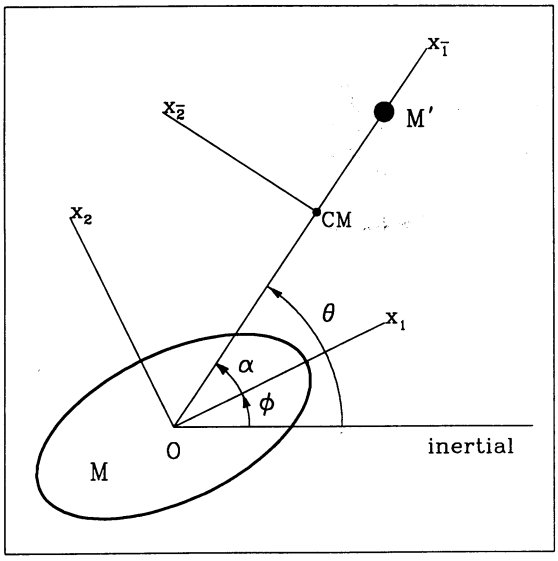

FIG. 3.—Sketch of the coordinate systems used for binaries

where $\rho(\boldsymbol{x})$ is the density distribution within M. To quadrupole order, we have

$$\frac{1}{|\boldsymbol{r}-\boldsymbol{x}|} \simeq \frac{1}{r} + \frac{\boldsymbol{x}\cdot\hat{\boldsymbol{r}}}{r^2} + \frac{1}{2r^3}\left[3(\boldsymbol{x}\cdot\hat{\boldsymbol{r}})^2 - x^2\right], \tag{5.4}$$

where $\hat{\boldsymbol{r}}$ is the unit vector connecting M to M'. Since $\int(\boldsymbol{x}\cdot\hat{\boldsymbol{r}})dm = 0$, we have

$$W_i = -\frac{GMM'}{r} - \frac{GM'}{2r^3}(3I_{rr} - I_{11} - I_{22} - I_{33}), \tag{5.5}$$

where

$$I_{rr} = \int d^3x\,\rho(\boldsymbol{x})(\boldsymbol{x}\cdot\hat{\boldsymbol{r}})^2 = I_{11}\cos^2\alpha + I_{22}\sin^2\alpha, \tag{5.6}$$

and I_{ii} is defined by equation (4.20). Combining equations (5.5) and (5.6), we obtain

$$W_i = -\frac{GMM'}{r} - \frac{GM'}{2r^3}\left[I_{11}(3\cos^2\alpha - 1) + I_{22}(3\sin^2\alpha - 1) - I_{33}\right]. \tag{5.7}$$

Given the Lagrangian (eqs. [5.1] and [5.2]), the dynamical equations can then be obtained from the Euler-Lagrange equations (2.13). Of particular interest are the equations for ϕ and θ. For $q_i = \phi$, we get

$$\frac{dJ_s}{dt} = \mathcal{N} = \frac{3GM'}{2r^3}(I_{11} - I_{22})\sin 2\alpha, \tag{5.8}$$

where J_s is the "spin" angular momentum of the star, given by equation (2.17), and $\mathcal{N}$ is the tidal torque exerted on the star. For $q_i = \theta$, equation (2.13) gives

$$\frac{dJ_{\rm orb}}{dt} = -\mathcal{N}, \tag{5.9}$$

where $J_{\rm orb} = \mu r^2\dot{\theta}$ is the orbital angular momentum. Thus we see that the total angular momentum,

$$J = J_s + J_{\rm orb}, \tag{5.10}$$

is conserved, as expected. Equation (2.13) for $q_i = \psi$ indicates that the fluid circulation given by equation (2.18) is also conserved, since tidal forces conserve the fluid vorticity.

The complete dynamical equations for a Roche-Riemann system in the absence of dissipation can be written as

$$\ddot{a}_1 = a_1(\Omega^2 + \Lambda^2) - 2a_2\Omega\Lambda - \frac{2\pi G}{q_n}a_1A_1\bar{\rho} + \left(\frac{5k_1}{n\kappa_n}\frac{P_c}{\rho_c}\right)\frac{1}{a_1} + \frac{GM'a_1}{r^3}(3\cos^2\alpha - 1), \tag{5.11}$$

$$\ddot{a}_2 = a_2(\Omega^2 + \Lambda^2) - 2a_1\Omega\Lambda - \frac{2\pi G}{q_n}a_2A_2\bar{\rho} + \left(\frac{5k_1}{n\kappa_n}\frac{P_c}{\rho_c}\right)\frac{1}{a_2} + \frac{GM'a_2}{r^3}(3\sin^2\alpha - 1), \tag{5.12}$$

$$\ddot{a}_3 = -\frac{2\pi G}{q_n}a_3A_3\bar{\rho} + \left(\frac{5k_1}{n\kappa_n}\frac{P_c}{\rho_c}\right)\frac{1}{a_3} - \frac{GM'a_3}{r^3}, \tag{5.13}$$

$$\frac{d}{dt}(a_1\Omega - a_2\Lambda) = -\dot{a}_1\Omega + \dot{a}_2\Lambda + \frac{3GM'a_1}{2r^3}\sin 2\alpha, \tag{5.14}$$

$$\frac{d}{dt}(-a_2\Omega + a_1\Lambda) = \dot{a}_2\Omega - \dot{a}_1\Lambda + \frac{3GM'a_2}{2r^3}\sin 2\alpha, \tag{5.15}$$

$$\ddot{r} = r\dot{\theta}^2 - \frac{G(M+M')}{r^2} - \frac{3\kappa_nG}{10}\frac{(M+M')}{r^4}\left[a_1^2(3\cos^2\alpha - 1) + a_2^2(3\sin^2\alpha - 1) - a_3^2\right], \tag{5.16}$$

$$\ddot{\theta} = -\frac{2\dot{r}\dot{\theta}}{r} - \frac{3\kappa_nG}{10}\frac{(M+M')}{r^5}(a_1^2 - a_2^2)\sin 2\alpha, \tag{5.17}$$

where $\dot{\theta} = \Omega_{\rm orb}$, $\dot{\phi} = \Omega$. For numerical integrations, equations (5.14) and (5.15) can be rewritten as

$$\dot{\Omega} = \left(\frac{a_2}{a_1} - \frac{a_1}{a_2}\right)^{-1}\left[2\left(\frac{\Omega}{a_2} + \frac{\Lambda}{a_1}\right)\dot{a}_1 - 2\left(\frac{\Omega}{a_1} + \frac{\Lambda}{a_2}\right)\dot{a}_2 - \frac{3GM'}{2r^3}\left(\frac{a_1}{a_2} + \frac{a_2}{a_1}\right)\sin 2\alpha\right], \tag{5.18}$$

$$\dot{\Lambda} = \left(\frac{a_2}{a_1} - \frac{a_1}{a_2}\right)^{-1}\left[2\left(\frac{\Omega}{a_1} + \frac{\Lambda}{a_2}\right)\dot{a}_1 - 2\left(\frac{\Omega}{a_2} + \frac{\Lambda}{a_1}\right)\dot{a}_2 - \frac{3GM'}{r^3}\sin 2\alpha\right]. \tag{5.19}$$

The pressure term in equations (5.11)–(5.13) can be handled in the same way as for a single star. It is easy to verify that equations (2.30) and (2.34) still apply.

6. DYNAMICAL INSTABILITY OF ROCHE-RIEMANN BINARIES

It is straightforward to show that, for an equilibrium system (i.e., when $\dot{a}_i = 0 = \ddot{a}_i$ and $\alpha = 0$), the dynamical equations (5.11)–(5.19) reduce to the equilibrium equations for Roche-Riemann binaries derived and solved in LRS1 (§ 8.1). We now examine the dynamical stability of the equilibrium solutions.

To study small dynamical oscillations, one could linearize the dynamical equations and calculate all the eigenfrequencies. This involves extensive algebra. However, we can show that the onset of dynamical instability is determined by a condition similar to equation (3.8), with an appropriately constructed energy function. For this purpose, it is convenient to use α instead of θ as an independent variable. Thus we define $\{q_i\} = \{a_1, a_2, a_3, r, \alpha, \phi, \psi\}$ here. The Lagrangian of the system as discussed in § 5 can be written as

$$L = \tfrac{1}{10}\kappa_n M(\dot{a}_1^2 + \dot{a}_2^2 + \dot{a}_3^2) + \tfrac{1}{2}I(\dot{\phi}^2 + \dot{\psi}^2) - \tfrac{2}{5}\kappa_n a_1 a_2 \dot{\phi}\dot{\psi} + \tfrac{1}{2}\mu\dot{r}^2 + \tfrac{1}{2}\mu r^2(\dot{\phi} + \dot{\alpha})^2 - U - W - W_i \,. \tag{6.1}$$

The canonical momenta associated with the $\{q_i\}$ are

$$P_{a_i} = \tfrac{1}{5}\kappa_n M\dot{a}_i \,, \qquad P_r = \mu\dot{r} \,, \qquad P_\alpha = \mu r^2(\dot{\phi} + \dot{\alpha}) \,, \qquad P_\phi = J \,, \qquad P_\psi = \mathscr{C} \,. \tag{6.2}$$

Because of the conservation of J and $\mathscr{C}$, and also because $\alpha = 0$ for an equilibrium configuration, it is convenient to define a subset of the variables $\{\alpha_i\} \equiv \{a_1, a_2, a_3, r\}$. The Hamiltonian can then be written as

$$H(\alpha_i, \alpha, P_{\alpha_i}, P_\alpha, J, \mathscr{C}) = \frac{1}{2(\kappa_n M/5)}(P_{a_1}^2 + P_{a_2}^2 + P_{a_3}^2) + \frac{1}{2\mu}P_r^2 + E(\alpha_i, \alpha, P_\alpha, J, \mathscr{C}) \,, \tag{6.3}$$

where

$$E(\alpha_i, \alpha, P_\alpha, J, \mathscr{C}) = \frac{1}{2\mu r^2}P_\alpha^2 + \frac{1}{2I_+}(J - P_\alpha + \mathscr{C})^2 + \frac{1}{2I_-}(J - P_\alpha - \mathscr{C})^2 + U + W + W_i \tag{6.4}$$

(compare with eq. [3.3]), where $I_\pm$ is defined in equation (3.4). Hamilton's equations $dP_{q_i}/dt = -\partial H/\partial q_i$ for $q_i = a_i$ give

$$\frac{1}{5}\kappa_n M\ddot{a}_i = -\left(\frac{\partial E}{\partial a_i}\right)_{P_\alpha, J, \mathscr{C}} = -\left(\frac{\partial E}{\partial a_i}\right)_{J,\mathscr{C}} + \dot{\alpha}\left(\frac{\partial P_\alpha}{\partial a_i}\right)_{J,\mathscr{C}} \,, \tag{6.5}$$

where for the second equality we have used $\partial E/\partial P_\alpha = \dot{\alpha}$, and we consider P_α to be a function of α_i, J, $\mathscr{C}$, and $\dot{\alpha}$, and E to be a function $E(\alpha_i, \alpha, \dot{\alpha}, J, \mathscr{C})$. Linearization of equation (6.5) about equilibrium, letting $\alpha_i = \alpha_{i,\mathrm{eq}} + \delta\alpha_i$, yields

$$\begin{aligned}\frac{1}{5}\kappa_n M\,\delta\ddot{a}_i &= -\sum_j \delta\alpha_j\left(\frac{\partial^2 E}{\partial a_i \partial\alpha_j}\right)_{\mathrm{eq}} - \alpha\left(\frac{\partial^2 E}{\partial a_i \partial\alpha}\right)_{J,\mathscr{C}} - \dot{\alpha}\left(\frac{\partial^2 E}{\partial a_i \partial\dot{\alpha}}\right)_{J,\mathscr{C}} + \dot{\alpha}\left(\frac{\partial P_\alpha}{\partial a_i}\right)_{J,\mathscr{C}} \\ &= -\sum_j \delta\alpha_j\left(\frac{\partial^2 E}{\partial a_i \partial\alpha_j}\right)_{\mathrm{eq}} - \dot{\alpha}\left(\frac{\partial^2 E}{\partial a_i \partial\dot{\alpha}}\right)_{J,\mathscr{C}} + \dot{\alpha}\left(\frac{\partial P_\alpha}{\partial a_i}\right)_{J,\mathscr{C}} \,,\end{aligned} \tag{6.6}$$

where the second equality follows because $(\partial^2 E/\partial a_i \partial\alpha) \propto \sin\alpha$ (see eq. [5.8]) and $|\alpha| \ll 1$ near equilibrium. Similarly, Hamilton's equation for $q_i = r$ yields

$$\mu\delta\ddot{r} = -\sum_j \delta\alpha_j\left(\frac{\partial^2 E}{\partial r \partial\alpha_j}\right)_{\mathrm{eq}} - \dot{\alpha}\left(\frac{\partial^2 E}{\partial r \partial\dot{\alpha}}\right)_{J,\mathscr{C}} + \dot{\alpha}\left(\frac{\partial P_\alpha}{\partial r}\right)_{J,\mathscr{C}} \,. \tag{6.7}$$

Now we substitute $\delta\alpha_i \propto e^{i\sigma t}$ in equations (6.6) and (6.7) and let $\sigma = 0$. We obtain

$$\sum_j \delta\alpha_j\left(\frac{\partial^2 E}{\partial\alpha_i \partial\alpha_j}\right)_{\mathrm{eq}} = 0 \qquad \text{for } \sigma = 0 \,. \tag{6.8}$$

Clearly, in this expression, E should be evaluated at $\alpha = 0$, the equilibrium value. Thus we can write $E = E(\alpha_i; J, \mathscr{C})$ with fixed $\alpha = 0$, and the onset of dynamical instability is determined from the condition

$$\det\left(\frac{\partial^2 E}{\partial\alpha_i \partial\alpha_j}\right)_{\mathrm{eq}} = 0 \,, \qquad i, j = 1, 2, \ldots \text{(onset of instability)} \,, \tag{6.9}$$

where the partial derivatives are evaluated holding J, $\mathscr{C}$ fixed. This condition forms the basis of the stability analysis of binary systems presented in LRS1 and LRS4. Although the new degree of freedom associated with α was not introduced in our previous analyses, the explicit derivation given above shows that the stability condition is not affected.

Alternatively, on quite general grounds, one can show that the stability conditions determined from equation (6.9) coincide with *turning points* along appropriately constructed equilibrium sequences (LRS1, § 2.3). Specifically, a dynamical stability limit coincides with the point where the total equilibrium energy and angular momentum are both minimum along a sequence with constant circulation. Using both methods (eq. [6.9] and the turning-point method), we have found in LRS1 (§ 9.2) that a Roche-Riemann binary can become dynamically unstable when the orbital separation is sufficiently small. This instability results from the strong tidal interaction, which can make the effective interaction potential between the two stars much steeper than $1/r$, thereby destabilizing a circular orbit (cf. Goldstein 1980, §§ 3–6; see also LRS2 for a qualitative discussion). The stability limits for various Roche-Riemann binary models have been tabulated in Tables 10 and 11 of LRS1.

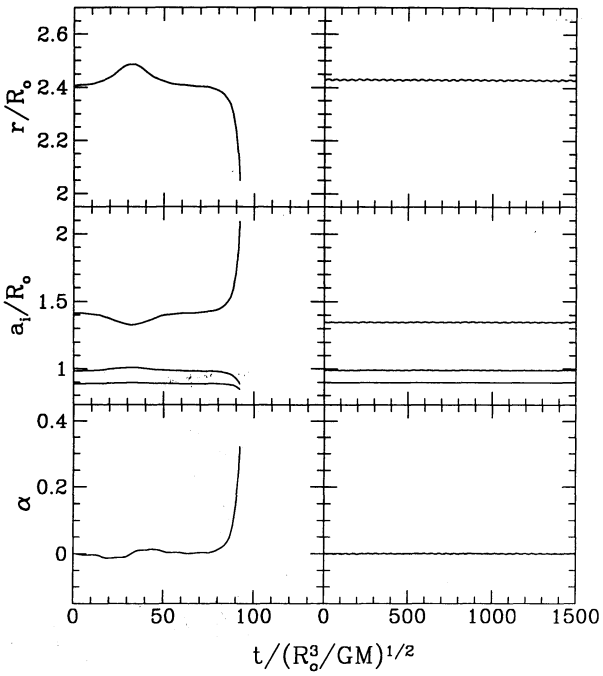

FIG. 4.—Evolution of the binary separation r, the axes a_i, and the lag angle α for Roche-Riemann binaries, with $p = M/M' = 1$ and $n = 1$. The initial configurations are in equilibrium, and corotating. The left-hand panels show the evolution of a dynamically unstable binary ($r/a_1 = 1.7$, $r/R_0 = 2.406$), while the right-hand panels show that of a stable binary ($r/a_1 = 1.8$, $r/R_0 = 2.427$). Both equilibrium configurations are perturbed by imposing a small radial velocity.

To illustrate how the instability develops, using our dynamical equations, we show in Figure 4 the time evolution of an unstable system with $n = 1$, $p = M/M' = 1$, and $\Lambda = 0$ (corotating). The dynamical equations were integrated numerically using a standard fifth-order Runge-Kutta scheme with adaptive step size (Press et al. 1992). At $t = 0$, an equilibrium solution is constructed for $r/a_1 = 1.7$, and $r/R_0 = 2.406$. This equilibrium solution is then perturbed by setting $\dot{r} = 10^{-3}(GM/R_0)^{1/2}$. For comparison, the results of an integration for a stable binary with $r/a_1 = 1.8$, $r/R_0 = 2.427$, and with the same applied perturbation, is also shown. The dynamical stability limit along the corotating (Roche) sequence with $n = 1$ and $p = 1$ is at $r/a_1 = 1.760$, or $r/R_0 = 2.417$. We see clearly in Figure 4 that, as the dynamical instability develops, a_1 increases while r decreases, and this is accompanied by the significant development of a tidal lag $\alpha > 0$. Of course, the precise evolution of an unstable binary depends on how the initial configuration is perturbed.

7. TIDAL CAPTURE AND DISRUPTION OF A STAR BY A MASSIVE BODY

Tidal interactions of stars and other fluid bodies have been discussed extensively in a number of different contexts. Fabian, Pringle, & Rees (1975) originally proposed that tidal encounters between a neutron star and a main-sequence star might lead to the formation of X-ray binaries in globular clusters (but see Rasio & Shapiro 1991; Kochanek 1992a; Rasio 1993). The first quantitative calculations of the orbital energy dissipation were performed by Press & Teukolsky (1977, hereafter PT) using a linear perturbation method. They were followed by many other studies using both linear theory (Lee & Ostriker 1986; McMillan, McDermott, & Taam 1987; Kochanek 1992a and references therein) and numerical hydrodynamic calculations (Rasio & Shapiro 1991). The tidal disruption of stars by a massive black hole can provide a mechanism for fueling low-luminosity active galactic nuclei (AGNs), and may also lead to observable flares in the luminosity of AGNs. Many aspects of this problem have been considered previously (Rees 1988; Evans & Kochanek 1989; Carter & Luminet 1985; Novikov, Pethick, & Polnarev 1992), including relativistic effects (Laguna et al. 1993). Tidal disruption of small bodies (planetesimals) by protoplanets has also been discussed in the context of the solar system formation (Boss, Cameron, & Benz 1991; Sridhar & Tremaine 1992).

The advantage of our ellipsoidal method for studying this problem is that it allows for the treatment of nonlinear effects, which are inevitable for close encounters. Using their affine stellar model, Carter & Luminet (1983; see also Luminet & Carter 1986) have studied in detail the tidal disruption of stars by massive black holes. Other studies using similar affine-type models include those of Kochanek (1992a), Kosovichev & Novikov (1992), and Sridhar & Tremaine (1992). There are several inconsistencies and differences in the results obtained in those previous studies. Thus we consider it worthwhile to reexamine the problem using our independent formulation of the dynamics, even though our equations are formally equivalent to those of the affine model. We include in some of our calculations the effects of fluid viscosity, which can be significant for the viscoelastic material in planetesimals (Sridhar & Tremaine 1992).

For definiteness, we focus on the encounter of a fluid body of mass M with a pointlike object of mass $M' \gg M$, and we consider only parabolic trajectories. A useful dimensionless parameter characterizing the encounter is

$$\eta = \left(\frac{M}{M + M'}\right)^{1/2}\left(\frac{r_p}{R_0}\right)^{3/2}, \tag{7.1}$$

where r_p is the periastron separation. The quantity η is simply the ratio of the timescale for the periastron passage, $\sim r_p/v_p$, where v_p is the velocity at the periastron, to the dynamical timescale of the star, $\sim R_0^{3/2}/(GM)^{1/2}$. When the relative velocity v_∞ between M and M' at infinite separation is nonzero, the orbit is slightly hyperbolic. However, as long as $v_p \gg v_\infty$, the trajectory remains very nearly parabolic close to periastron, where the tidal interaction is strongest.

7.1. *Dynamical Calculations for Compressible Ellipsoids*

For a given η, we integrate equations (5.11)–(5.19) numerically to determine the dynamical effects of the tidal interaction. Initially the star is placed on a parabolic orbit, far away from the massive body ($r/R_0 \gg \eta^{2/3}p^{-1/3}$), and it is assumed to be spherical (nonrotating). To avoid the singularity in equations (5.18) and (5.19) when $a_1 = a_2$, the initial configuration is slightly perturbed by increasing (decreasing) a_1 (a_2) by $\sim 0.1\%$. We have checked that the final numerical results (including the energy transfer) are independent of the exact amplitude of this initial perturbation. The total angular momentum, fluid circulation, and energy are conserved to very high accuracy throughout the evolution (typical error $\lesssim 10^{-7}$). For $n = 0$ we also check the conservation of the volume: the product $a_1 a_2 a_3$ remains constant to within $\sim 10^{-7}$ typically. For most calculations we use $M'/M = 10^6$, but the results are essentially independent of the exact value as long as $M'/M \gtrsim 10^3$.

Typical results are illustrated in Figure 5 for an encounter with $\eta = 2.8$ and $n = 1.5$. Here $t = 0$ corresponds to the time of periastron passage. After the encounter, the star becomes an oscillating Riemann-S ellipsoid with zero fluid circulation, but finite angular momentum. The angular momentum deposited in the star through the tidal interaction does not lead to uniform spin in the absence of fluid viscosity.

7.2. *Energy and Angular Momentum Transfer in the Linear Theory*

The energy transferred from the orbit to the star during a tidal encounter can be calculated exactly in the limit of linear perturbations using the theory developed by Press & Teukolsky (1977). Here we also calculate the corresponding transfer of angular momentum using the same formalism.

The amount of energy transferred can be written as

$$\Delta E = -\int dt \int d^3x\, \rho \frac{\partial \boldsymbol{\xi}}{\partial t} \cdot \nabla \mathcal{U} , \tag{7.2}$$

where $\mathcal{U}$ is the gravitational potential of the point mass, $\mathcal{U}(\boldsymbol{x}, t) = -GM'/|\boldsymbol{x} - \boldsymbol{r}|$, with $\boldsymbol{r}$ describing the orbital trajectory and $\boldsymbol{x}$ specifying the position of a fluid element inside M. The Lagrangian displacement $\boldsymbol{\xi}$ of a fluid element in the star is assumed to be small, and can be decomposed into normal eigenmode components $\boldsymbol{\xi}_{nlm}$, where $\{n, l, m\}$ are indices specifying the eigenmodes. An important quantity in any discussion of tidal interactions is the dimensionless coefficient characterizing the coupling between the tidal potential and a particular normal mode (Zahn 1970; PT),

$$Q_{nl} = \int d^3x\, \rho \boldsymbol{\xi}^*_{nlm} \cdot \nabla[r^l Y_{lm}(\theta, \phi)] = \int_0^R \rho l r^{l+1}\, dr[\xi^r{}_{nl}(r) + (l+1)\xi^\perp{}_{nl}(r)] , \tag{7.3}$$

where, for spheroidal modes, we have expressed $\boldsymbol{\xi}_{nlm}$ as a sum of radial and tangential components,

$$\boldsymbol{\xi}_{nlm}(\boldsymbol{r}) = [\xi^r{}_{nl}(r)\boldsymbol{e}_r + r\xi^\perp{}_{nl}(r)\nabla] Y_{lm}(\theta, \phi) . \tag{7.4}$$

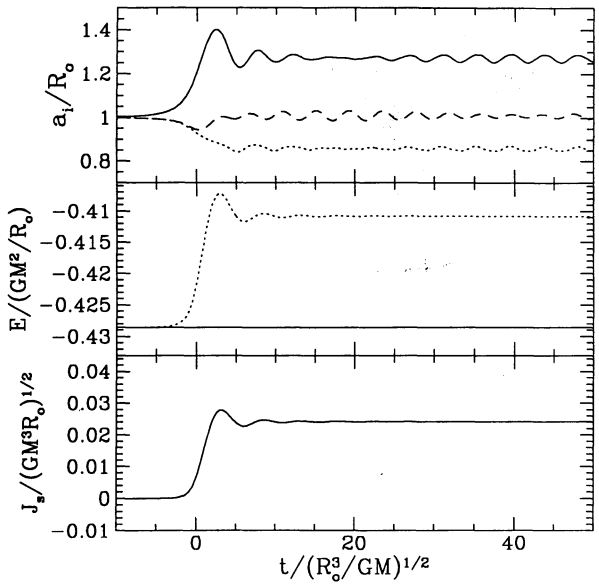

FIG. 5.—Evolution of the axes, energy, and angular momentum of a star with $n = 1.5$ during a parabolic encounter with a massive ($M' \gg M$) body. The parameter η is equal to 2.8 (eq. [7.1]). The solid line in the middle shows the total (conserved) energy in the system.

The normal modes ξ_{nlm} are normalized so that $\int d^3x\,\rho\boldsymbol{\xi}_{nlm}\cdot\boldsymbol{\xi}_{n'l'm'}=\delta_{nn'}\delta_{ll'}\delta_{mm'}$. The total energy transfer during a parabolic encounter can be written (PT)

$$\Delta E=\frac{GM'^2}{R_0}\sum_{l=2}^{\infty}\left(\frac{R_0}{r_p}\right)^{2l+2}T_l(\eta)\,, \tag{7.5}$$

where the dimensionless function T_l is given by

$$T_l(\eta)=2\pi^2\sum_n|Q_{nl}|^2\sum_{m=-1}^{l}|K_{nlm}|^2\,. \tag{7.6}$$

The function K_{nlm} involves the eigenfrequencies ω_{nl} and is given in PT.

The angular momentum transfer during an encounter is given by

$$\Delta J_z=\int dt\int d^3x(\rho+\delta\rho)\tau_z=\int dt\int d^3x\,\delta\rho\left(-\frac{\partial\mathcal{U}}{\partial\phi}\right), \tag{7.7}$$

where $\delta\rho=-\nabla\cdot(\rho\boldsymbol{\xi})$ is the Eulerian perturbation of the fluid density in the star, and $\tau_z=-\partial\mathcal{U}/\partial\phi$ is the tidal torque per unit mass. Using a similar procedure to that in PT, we obtain (Lai 1994b)

$$\Delta J_z=\frac{GM'^2}{R_0}\left(\frac{GM}{R_0^3}\right)^{-1/2}\sum_{l=2}^{\infty}\left(\frac{R_0}{r_p}\right)^{2l+2}S_l(\eta)\,, \tag{7.8}$$

where the dimensionless function S_l is given by

$$S_l(\eta)=2\pi^2\sum_n\frac{|Q_{nl}|^2}{\omega_{nl}}\sum_{m=-l}^{l}(-m)|K_{nlm}|^2\,. \tag{7.9}$$

Note that K_{nlm} is larger for $m=-2$; thus ΔJ_z in equation (7.8) is positive. Also note that contributions to ΔE and to ΔJ from different terms in the sum are related by $\Delta J_{nlm}=(-m/\omega_{nl})\Delta E_{nlm}$.[6]

In the incompressible limit ($n=0$ and $\Gamma=\Gamma_1=\infty$), only f-modes of oscillation exist. These have eigenfrequencies $\omega_{0l}^2/(GM/R^3)=2l(l-1)/(2l+1)$ (see, e.g., Cox 1980). For the dominant $l=2$ quadrupole modes (including the Kelvin mode; cf. § 3.3), $\omega_{02}^2/(GM/R^3)=\frac{4}{5}$. The normalized eigenfunctions are $\xi^r{}_{02}=2\xi^{\perp}{}_{02}=(8\pi/3)^{1/2}r$, for which we have $Q_{02}=(3/2\pi)^{1/2}MR^2$.

7.3. *Large-η Encounters: Comparison with Linear Theory*

In Figure 6 we compare our ellipsoidal results for the energy and angular momentum transfer (§ 7.1) with those of linear theory. In the limit where $\eta\gg1$, the linear theory should be exact. The three values of n we have considered are $n=0$, 1.5, and 2.5. For $n=0$, one would expect the results from the two methods to agree precisely, since only the f-modes are involved in the linear theory, and the $l=2$ quadrupole interaction is the leading order (the $l=2$ mode structure obtained from the two methods is the same; see § 3.3). We find that this is not the case, i.e., even in the limit of $\eta\to\infty$, the results from the two methods do not agree. The same conclusion was reached by Kosovichev & Novikov (1992). Kochanek (1992a) considered only $n=1.5$ and concluded that the discrepancy was probably due to small errors in the numerical integration of his affine-model equations. Kosovichev & Novikov (1992) attributed the discrepancy to slight deviations of the true f-mode displacement from an exact ellipsoid. They argued that, in an ellipsoidal model, the stellar shape is too prolate, leading to stronger tidal interaction. We question the validity of this interpretation, since for a circular binary in equilibrium it can be shown explicitly that the energy shifts obtained from the linear theory and from the ellipsoidal (Roche-Riemann) model are identical (Lai 1994b). Note, however, from Figure 6, that the difference in the amount of energy dissipated is less than 40%. The resulting tidal capture radius is therefore hardly affected, since the dependence of ΔE on r_p is extremely steep.

In the compressible cases ($n>0$), other types of nonradial oscillation modes, which are absent in the ellipsoidal model, can be excited by the tidal iteraction. As discussed in § 2.1, the ellipsoidal model incorporates only the $l=2$ f-modes of oscillation. In general, p-modes are also excited, and, if $\Gamma_1>\Gamma$, one should also include g-modes. However, the coupling coefficients Q_{nl} (eq. [7.3]) of the p-modes and g-modes are typically much smaller than that of the f-modes (Lee & Ostriker 1986). When g-modes exist ($\Gamma_1>\Gamma$), their contribution to the tidal energy transfer is larger than that of the f-modes at large separation (see the dotted lines in Fig. 6). The reason is that at larger separation, "resonances" occur since the (very low) frequency of the tidal driving force is always close to that of some high-order g-mode. These resonances lead to a more efficient energy transfer at large separation.

7.4. *Close Encounters: The Tidal Disruption Limit*

As η decreases, the amplitude of the tidal perturbations increases and linear theory eventually breaks down. Below the tidal *disruption limit* at some critical $\eta=\eta_{\rm dis}$, the amount of energy transferred to the star exceeds its original binding energy (the stellar energy E_s, eq. [2.26], becomes positive), and the star is left unbound after the encounter. In Figure 7 we show the results of two calculations for $n=1.5$. For one encounter we used $\eta=1.85$, slightly larger than the disruption limit $\eta_{\rm dis}=1.84$, and for the other we used $\eta=1.83<\eta_{\rm dis}$, the star remains bound after the periastron passage, although the axes experience large-amplitude nonlinear oscillations when η is very close to $\eta_{\rm dis}$. For $\eta<\eta_{\rm dis}$, the star becomes unbound ($E_s>0$); at least one of the axes keeps increasing monotonically in time after the encounter, leading to a progressively more and more elongated structure. This behavior is identical to that found by Kosovichev & Novikov (1992) for $n=0$.

[6] In eqs. (7.6) and (7.9), the index m does not correspond to the original mode index in Y_{lm}. Instead, contributions from $m=2$ and $m=-2$ modes have been regrouped to derive these final expressions. In fact, it can be shown that the $m=2$ and $m=-2$ modes contribute to the tidal energy and angular momentum equally.

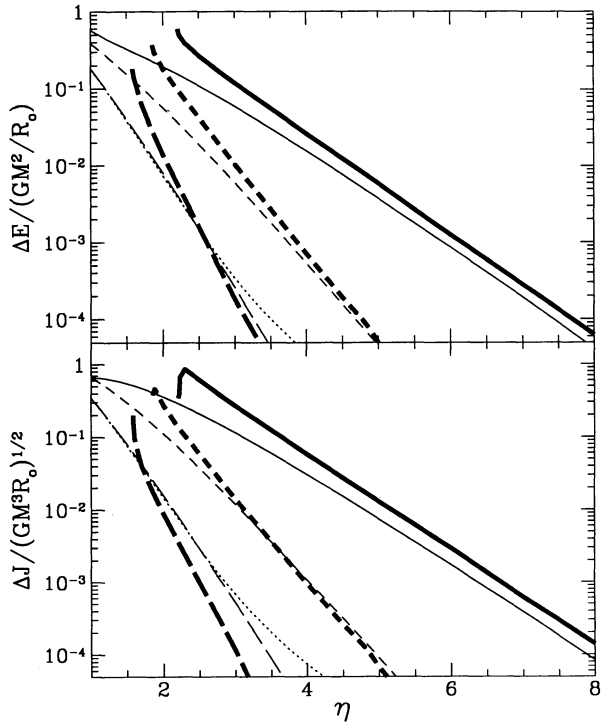

FIG. 6

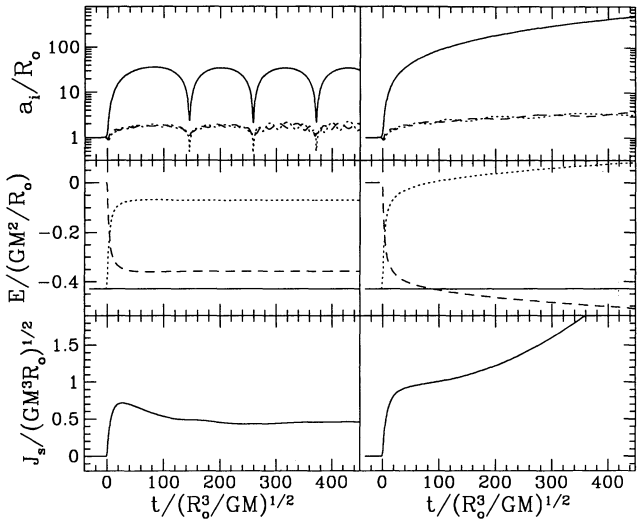

FIG. 7

FIG. 6.—Energy transfer and angular momentum transfer to the star during its parabolic encounter with a massive body. The heavy lines are the results obtained by integrating our equations numerically for a compressible ellipsoid, while the lighter lines show the results of linear perturbation theory (eqs. [7.5] and [7.8]). The solid lines are for $n = 0$, the short-dashed lines for $n = 1.5$, and the long-dashed lines for $n = 2.5$. In the linear theory, all modes are calculated assuming $\Gamma_1 = \Gamma$, except in the case of $n = 2.5$, where we have also included curves (*dotted lines*) showing the results when $\Gamma_1 = 5/3$.

FIG. 7.—Same as Fig. 5, but for $\eta = 1.85 > \eta_{dis}$ (*left*) and $\eta = 1.83 < \eta_{dis}$ (*right*). The dashed lines in the middle show the orbital energy.

In Table 2 we list the values of η_{dis} for different polytropic indices. For $n = 0$ our results agree precisely with those of Kosovichev & Novikov (1992) and Sridhar & Tremaine (1992) but not with those of Luminet & Carter (1986). For larger n, r_{dis} decreases, since the tidal interaction is less effective for more centrally concentrated objects. For comparison, we also list in Table 2 the absolute *Roche-Riemann limit*, η_{RR}, which corresponds to the minimum separation for an equilibrium configuration, among all Roche-Riemann binaries, to exist in a circular orbit (see LRS1, § 8.2). Note that the Roche limit for corotating binaries, as well as the irrotational Roche-Riemann limit for $\mathscr{C} = 0$ binaries (LRS3), all correspond to larger separations than η_{RR}. From Table 2 we see that, for all cases $\eta_{RR} > \eta_{dis}$, which is intuitively expected.

We note that even when $\eta > \eta_{dis}$, the object can become highly elongated (see Fig. 7), with $a_1 \gg a_2, a_3$, even though on simple energetic grounds it is still bound. In reality, such a needle-like object is likely to be subject to the "sausage" instability of infinite cylinders (Chandrasekhar 1961) and would break up into small pieces. Of course, our ellipsoidal model is not capable of treating this process.

7.5. *Effects of Viscosity*

Viscous dissipation forces can be easily incorporated into the dynamical equations (5.11)–(5.19). Since the motion of the center of mass of the star is not affected by viscous dissipation (which depends only on the shear stresses inside the star), the viscous forces

TABLE 2

DISRUPTION LIMITS AND ROCHE-RIEMANN LIMITS[a]

n	η_{dis}	η_{RR}
0	2.21	3.806
0.5	2.08	3.427
1.0	1.96	3.054
1.5	1.84	2.698
2.0	1.71	2.368
2.5	1.584	2.117

[a] Here η_{dis} is the disruption limit for encounters between a star and a massive body, and η_{RR} is the Roche-Riemann limit for equilibrium binaries in circular orbits.

derived for an isolated star (§ 4.1) can be directly applied to binaries. The dynamical equations (5.11)–(5.15) are modified in exactly the same way as in equations (4.10)–(4.16) for single stars. Also, since $\mathscr{F}_r = \mathscr{F}_\theta = 0$, equations (5.16) and (5.17) remain unchanged. We assume that $\bar{\nu}$ is a constant during the dynamical evolution.

Typical results are illustrated in Figure 8. Here the fluid viscosity has the value $\bar{\nu} = 0.01\ (GMR_0)^{1/2}$. We find that the disruption limit $\eta_{\rm dis}$ is smaller than in the inviscid case. For $\eta > \eta_{\rm dis} \simeq 1.72$, the star is still bound after the encounter ($E_s < 0$). Comparing with Figure 7, we see that the fluid viscosity damps out the large-amplitude, nonlinear oscillations of the ellipsoid after the encounter. Since the fluid circulation is not conserved in the presence of viscosity, the fluid does *not* remain irrotational. Instead, because viscous forces tend to damp out the differential rotation (i.e., $\Lambda \to 0$ after the encounter), the star evolves to become an equilibrium Jacobi ellipsoid on the viscous dissipation timescale. This is very different from the undamped, inviscid case. When the post encounter stellar energy E_s is positive, as in the case where $\eta = 1.71$ in Figure 8, the star becomes unbound, with one of the axes increasing monotonically. This is similar to what we found in the inviscid case.

In Figure 9 we show the disruption limits as a function of the fluid viscosity for three values of n. The maximum physical value for the viscosity is $\bar{\nu} \approx (GMR_0)^{1/2}$, corresponding to momentum transport across the whole star in a dynamical timescale. In all cases, the disruption limit of a viscous body is smaller than that of an inviscid body, as a result of the viscous damping of kinetic energy. This result is in agreement with the conclusions reached by Sridhar & Tremaine (1992). Note, however, that the reduction of $\eta_{\rm dis}$ is significant only for very large viscosities, $\bar{\nu} \gtrsim 10^{-2}(GMR_0)^{1/2}$. Typical viscosities in stars (even the large turbulent viscosity in convective envelopes) always remain $\lesssim 10^{-4}(GMR_0)^{1/2}$.

8. SECULAR EVOLUTION OF BINARIES DRIVEN BY VISCOSITY

As discussed in § 7.5, the viscous dissipation forces can be easily incorporated into the dynamical equations for the binaries. In this section we consider the secular evolution driven by viscous dissipation of a binary in a circular orbit. This subject has been well studied in the literature (see, e.g., Goldreich & Peale 1968 for a review). The basic ingredients were already established in the weak friction theory developed by G. Darwin more than a century ago. Our purpose in this section is to consider some aspects of this classical astronomical problem in the context of our compressible ellipsoid model, which naturally extends the early treatments to the nonlinear regime.

8.1. *Tidal Lag Angle Due to Viscosity*

Our present understanding of the tidal evolution of binary systems is largely based on the weak friction model. In this model, the viscosity of the star induces a lag angle between the static tidal bulge and the direction to the companion. This results in a torque and angular momentum transfer between the spin of the star and the orbit. This mechanism can lead to synchronization of the spin with the orbital motion, and a corresponding evolution of the binary orbit. Any degree of nonsynchronization is necessarily associated with a tidal lag angle, given by

$$\alpha \sim \frac{\Delta\Omega}{\omega_0^2 t_{\rm visc}} \sim \frac{\bar{\nu} R\, \Delta\Omega}{GM}, \tag{8.1}$$

where $\Delta\Omega = \Omega - \Omega_s$, $\omega_0 \sim (GM/R^3)^{1/2}$ is the fundamental frequency of the star, and $t_{\rm visc} \sim R^2/\nu$ is the viscous dissipation time.

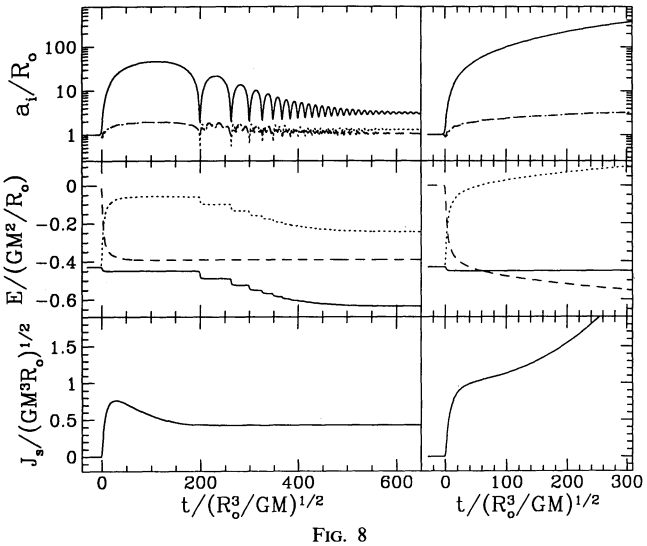

FIG. 8

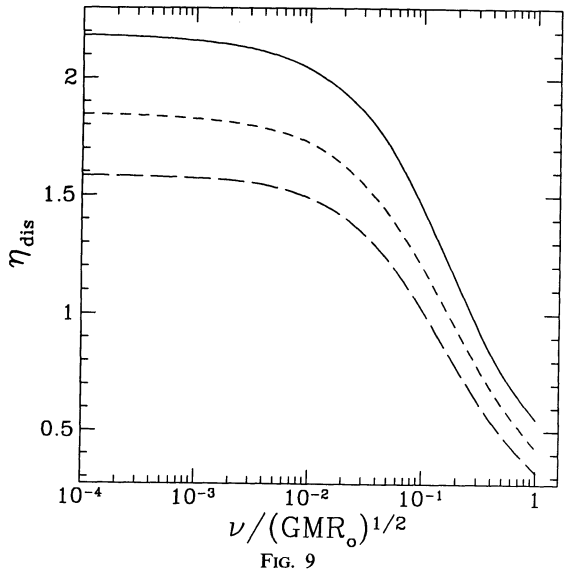

FIG. 9

FIG. 8.—Same as Fig. 7, but here the viscosity is nonzero, with $\nu = 0.01(GMR_0)^{1/2}$. On the left $\eta = 1.73 > \eta_{\rm dis}$, and on the right $\eta = 1.71 < \eta_{\rm dis}$.

FIG. 9.—Disruption limit $\eta_{\rm dis}$ for the parabolic encounter of a star with a massive body, as a function of the fluid viscosity ν. The viscosity is assumed to be constant during the encounter. The three curves correspond to $n = 0.1$ (*solid line*), $n = 1.5$ (*short-dashed line*), and $n = 2.5$ (*long-dashed line*).

We can easily derive the exact result in the limit of large binary separation using our ellipsoidal model. For large r/R we have $a_1 \simeq a_2$, so that $J_s \simeq -\mathscr{C}$ (see eqs. [2.17] and [2.18]). Using equation (5.8) for dJ_s/dt and $d\mathscr{C}/dt = -\bar{\nu}M\Lambda(a_1^2 - a_2^2)^2/(a_1 a_2)^2$ (see eq. [4.9]), we find

$$\sin 2\alpha \simeq \bar{\nu}\Lambda \frac{10r^3}{3\kappa_n GM'R^2}\left(\frac{a_1^2 - a_2^2}{a_1 a_2}\right). \tag{8.2}$$

For large r we have

$$\frac{a_1^2 - a_2^2}{a_1 a_2} \simeq \frac{15}{2} q_n \frac{M'}{M}\left(\frac{R}{r}\right)^3, \tag{8.3}$$

(see eq. [A25] in LRS4), and the tidal lag becomes

$$\alpha \simeq \frac{10}{4}(5 - n)\frac{\bar{\nu}\Lambda R}{GM}, \tag{8.4}$$

providing the coefficient of proportionality in equation (8.1) (recall that $\Lambda \simeq \Omega - \Omega_s$).

8.2. *Viscous Evolution*

In the presence of viscosity, only synchronized binaries can be in true equilibrium. Any degree of nonsynchronization necessarily leads to evolution. However, when the viscosity is sufficiently small, the binaries evolve slowly along a sequence of quasi-equilibrium configurations. Thus, in most cases, dynamical calculations are not needed to follow the viscous evolution. Since the viscous forces conserve angular momentum, the binary evolution driven by viscosity proceeds along sequences of constant total angular momentum J. This has been discussed extensively in LRS4 (§ 6). Depending on the value of J, the final fate of the binary can be qualitatively different. Consider the example in Figure 10, where we show the variation of the total energy along three different equilibrium sequences: one is the corotating sequence, and the other two have constant J. All three sequences are for $n = 0$ and $M/M' = 1$. A critical angular momentum $J = J_{\rm crit}$ is the minimum angular momentum along the corotating sequence. When $J > J_{\rm crit}$, the constant-J curve intersects the corotating curve, at two points corresponding to the minimum or maximum of the energy along the constant-J sequence. For $J < J_{\rm crit}$, no configuration along the constant-J sequence lies on the corotating sequence. Clearly, for $J > J_{\rm crit}$ the viscous forces drive the binary toward a stable corotating configuration, while for $J < J_{\rm crit}$ the viscous forces drive

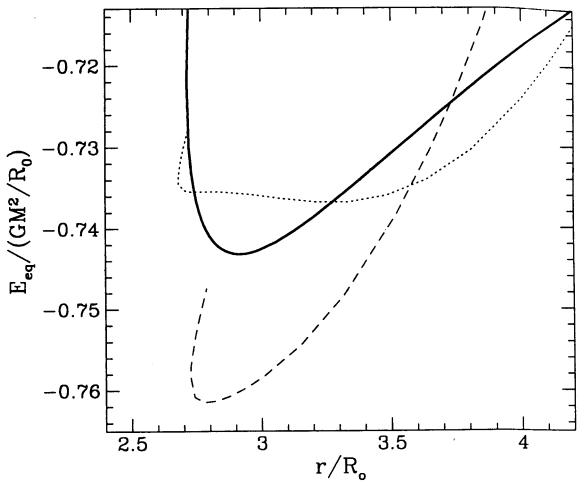

FIG. 10

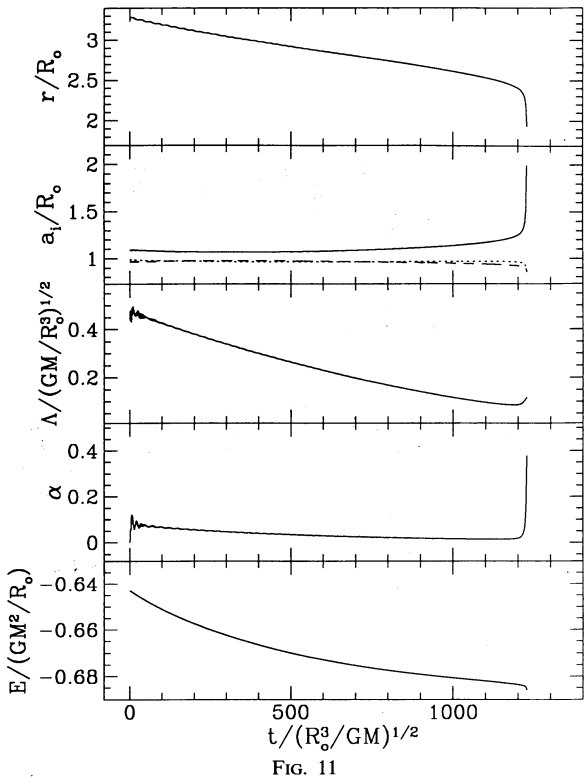

FIG. 11

FIG. 10.—Total energy $E_{\rm eq}$ of several equilibrium Roche-Riemann sequences for $p = M/M' = 1$ and $n = 0$, as a function of the binary separation r. The solid line is for the corotating sequence ($\Lambda = 0$), the dotted line for a sequence with constant $\bar{J} = J/(GM^3R_0)^{1/2} = 1.4 > \bar{J}_{\rm crit} = 1.375$, and the dashed line for a sequence with constant $\bar{J} = 1.3 < \bar{J}_{\rm crit}$.

FIG. 11.—Evolution of a Roche-Riemann binary driven by viscosity. Here $p = 1$, $n = 1$, and $\nu = 0.01(GMR_0)^{1/2}$. The initial configuration is an equilibrium Roche-Riemann binary with $f_R = -4$ and $r/a_1 = 3$, corresponding to $J = 1.220(GM^3R_0)^{1/2}$. Here r is the binary separation, a_i are the ellipsoid's axes, Λ measures the degree of nonsynchronization ($\Lambda \simeq \Omega - \Omega_s$), α is the tidal lag angle, and E is the total energy of the system.

orbital decay to final coalescence. More detailed discussions of these points can be found in LRS4. Values of $J_{\rm crit}$ for general n and p can be found in Table 10 of LRS1.

When a dynamical instability is encountered during secular orbital decay, dynamical calculations are needed to follow the subsequent evolution. In Figure 11 we show an example of such a dynamical calculation. Here $p = M/M' = 1$, $n = 1$, and the viscosity $\bar{\nu} = 0.01(GMR_0)^{1/2}$ is assumed to be constant throughout the evolution. The initial state is constructed by solving the equations for an equilibrium Roche-Riemann configuration with $f_{\rm R} \equiv -\Lambda(a_1^2 + a_2^2)/(\Omega a_1 a_2) = -4$ and $r/a_1 = 3$ (LRS1, § 8), corresponding to a total angular momentum $J = 1.220$. We set $\alpha = 0$ at $t = 0$. After a transient oscillation, α attains a small but finite value, corresponding to the tidal lag derived in § 8.1. The reason is that, as mentioned before, in the presence of viscosity, the binary is not exactly in equilibrium state, and viscosity-induced tidal lag is inevitable. During the secular evolution, the binary stays very close to an equilibrium evolution track with constant J. However, as the dynamical stability limit is approached, the evolution becomes much faster, and a large *dynamical* tidal lag develops. This dynamical behavior is similar to that shown in Figure 4.

9. BINARY EVOLUTION DRIVEN BY THE GRAVITATIONAL RADIATION REACTION

In this section we incorporate the gravitational radiation reaction in our dynamical equations for binaries. This allows us to study binary coalescence driven by the emission of gravitational waves. The equations are derived in § 9.1. In § 9.2 we consider the coalescence of a Roche-Riemann binary. In particular, we study how the dynamical instability (§ 6) is approached as the binary orbit decays.

The most important astrophysical applications of these results concern the coalescence of close binaries containing two compact objects. Coalescing neutron star binaries have long been recognized as promising sources of gravitational radiation that should become detectable with the new generation of laser interferometers such as LIGO (Abramovici et al. 1992). They may also be sources of extragalactic gamma-ray bursts (Paczyński 1986; Eichler et al. 1989). Coalescing white dwarf binaries are now thought to be the likely progenitors of Type Ia supernovae (Yungelson et al. 1994 and references therein), and they are also important sources of low-frequency gravitational waves that should be easily detectable by future space-based interferometers (Evans, Iben, & Smarr 1987). In § 9.2 below, we present a simple application to the case of a coalescing neutron star–black hole system (which can be modeled as a Roche-Riemann binary). Applications to double neutron star systems will be presented in detail elsewhere (Lai & Shapiro 1994b).

9.1. *Dynamical Equations Including the Gravitational Radiation Reaction*

To calculate the gravitational radiation reaction forces, we consider two coordinate systems (see Fig. 3): the *body coordinate system*, centered on M, with basis vectors $\{\boldsymbol{e}_i\}$ spanning the principal axes, and the *orbital coordinate system*, centered at the CM of the system, with basis vectors $\{\boldsymbol{e}_{\bar{i}}\}$; $\boldsymbol{e}_{\bar{1}}$ is along the line joining M and M', $\boldsymbol{e}_{\bar{2}}$ is perpendicular to $\boldsymbol{e}_{\bar{1}}$ in the orbital plane, and $\boldsymbol{e}_{\bar{3}}$ is perpendicular to the orbital plane. The two coordinate systems are related by

$$\begin{aligned} x_{\bar{1}} &= x_1 \cos\alpha + x_2 \sin\alpha - r_{\rm cm} , \\ x_{\bar{2}} &= -x_1 \sin\alpha + x_2 \cos\alpha , \\ x_{\bar{3}} &= x_3 . \end{aligned} \tag{9.1}$$

We now write the gravitational radiation back-reaction potential as

$$\Phi_{\rm react} = \frac{G}{5c^5} \mathcal{I}^{(5)}_{\bar{i}\bar{j}} x_{\bar{i}} x_{\bar{j}} . \tag{9.2}$$

This has the same form as equation (4.17), except that here we have used a different coordinate system: $\mathcal{I}^{(5)}_{\bar{i}\bar{j}}$ is the fifth derivative of the reduced quadrupole moment tensor of the system *projected onto the orbital frame*. Expressions for $\mathcal{I}^{(5)}_{\bar{i}\bar{j}}$ are derived in the Appendix.

For M' the velocity is simply

$$\boldsymbol{v}' = \dot{r}'_{\rm cm} \boldsymbol{e}_{\bar{1}} + \Omega_{\rm orb} r'_{\rm cm} \boldsymbol{e}_{\bar{2}} , \tag{9.3}$$

where $r'_{\rm cm}$ is the distance between the CM and M'. Thus the contribution to the dissipation function from M' is

$$\mathcal{W}_{M'} = -\frac{2G}{5c^5} [M' r'_{\rm cm} \dot{r}'_{\rm cm} \mathcal{I}^{(5)}_{\bar{1}\bar{1}} + M' r'^2_{\rm cm} \Omega_{\rm orb} \mathcal{I}^{(5)}_{\bar{1}\bar{2}}] . \tag{9.4}$$

The fluid velocity in M can be written as

$$\boldsymbol{v} = \boldsymbol{u} + \boldsymbol{u}_{\rm orb} = u_i \boldsymbol{e}_i + (-\dot{r}_{\rm cm} \boldsymbol{e}_{\bar{1}} - \Omega_{\rm orb} r_{\rm cm} \boldsymbol{e}_{\bar{2}}) , \tag{9.5}$$

where $\boldsymbol{u}$ is the fluid velocity relative to the CM of M and $\boldsymbol{u}_{\rm orb}$ is the orbital velocity. From equations (2.2)–(2.4), we have

$$\begin{aligned} u_1 &= \frac{\dot{a}_1}{a_1} x_1 + \left(\frac{a_1}{a_2}\Lambda - \Omega\right) x_2 , \\ u_2 &= \frac{\dot{a}_2}{a_2} x_2 + \left(-\frac{a_2}{a_1}\Lambda + \Omega\right) x_1 , \\ u_3 &= \frac{\dot{a}_3}{a_3} x_3 . \end{aligned} \tag{9.6}$$

Therefore,

$$\boldsymbol{v}\cdot\nabla\Phi_{\rm react}=[u_k\boldsymbol{e}_k+\boldsymbol{u}_{\rm orb}]\cdot\frac{2G}{5c^5}I^{(5)}_{\bar{i}\bar{j}}x_{\bar{j}}\boldsymbol{e}_{\bar{i}}\,. \tag{9.7}$$

Using equation (9.5) and the relation between $\{\boldsymbol{e}_i\}$ and $\{\boldsymbol{e}_{\bar{i}}\}$, we get

$$\boldsymbol{v}\cdot\nabla\Phi_{\rm react}=\frac{2G}{5c^5}\left[u_1x_{\bar{j}}(I^{(5)}_{\bar{1}\bar{j}}\cos\alpha-I^{(5)}_{\bar{2}\bar{j}}\sin\alpha)+u_2x_{\bar{j}}(I^{(5)}_{\bar{1}\bar{j}}\sin\alpha+I^{(5)}_{\bar{2}\bar{j}}\cos\alpha)+u_3x_{\bar{j}}I^{(5)}_{\bar{3}\bar{j}}-\dot{r}_{\rm cm}x_{\bar{j}}I^{(5)}_{\bar{1}\bar{j}}-r_{\rm cm}\Omega_{\rm orb}x_{\bar{j}}I^{(5)}_{\bar{2}\bar{j}}\right]. \tag{9.8}$$

Substituting equations (9.1) and (9.6) in this expression, integrating over the mass distribution in M, and adding the contribution from M' (eq. [9.4]), we obtain the total dissipation rate

$$\begin{aligned}\mathscr{W}&=\mathscr{W}_M+\mathscr{W}_{M'}=-\int_M\boldsymbol{v}\cdot\nabla\Phi_{\rm react}\,dm+W_{M'}\\&=-\frac{2G}{5c^5}\left(\frac{1}{5}\kappa_nM\right)\Big\{(I^{(5)}_{\bar{1}\bar{1}}\cos^2\alpha+I^{(5)}_{\bar{2}\bar{2}}\sin^2\alpha-I^{(5)}_{\bar{1}\bar{2}}\sin 2\alpha)a_1\dot{a}_1+(I^{(5)}_{\bar{1}\bar{1}}\sin^2\alpha+I^{(5)}_{\bar{2}\bar{2}}\cos^2\alpha+I^{(5)}_{\bar{1}\bar{2}}\sin 2\alpha)a_2\dot{a}_2+I^{(5)}_{\bar{3}\bar{3}}a_3\dot{a}_3\\&\quad+\left[I^{(5)}_{\bar{1}\bar{2}}\cos 2\alpha+(I^{(5)}_{\bar{1}\bar{1}}-I^{(5)}_{\bar{2}\bar{2}})\frac{1}{2}\sin 2\alpha\right](a_1^2-a_2^2)\Omega\Big\}-\frac{2G}{5c^5}\mu(I^{(5)}_{\bar{1}\bar{1}}r\dot{r}+I^{(5)}_{\bar{1}\bar{2}}r^2\Omega_{\rm orb})\,,\end{aligned} \tag{9.9}$$

where we have used equation (4.20) and $Mr_{\rm cm}^2+M'r_{\rm cm}'^2=\mu r^2$.

Using equation (4.21), the dissipative forces are then given by

$$\begin{aligned}\mathscr{F}_{a_1}&=-\frac{2G}{5c^5}\left(\frac{1}{5}\kappa_nM\right)(I^{(5)}_{\bar{1}\bar{1}}\cos^2\alpha+I^{(5)}_{\bar{2}\bar{2}}\sin^2\alpha-I^{(5)}_{\bar{1}\bar{2}}\sin 2\alpha)a_1\,,\\\mathscr{F}_{a_2}&=-\frac{2G}{5c^5}\left(\frac{1}{5}\kappa_nM\right)(I^{(5)}_{\bar{1}\bar{1}}\sin^2\alpha+I^{(5)}_{\bar{2}\bar{2}}\cos^2\alpha+I^{(5)}_{\bar{1}\bar{2}}\sin 2\alpha)a_2\,,\\\mathscr{F}_{a_3}&=-\frac{2G}{5c^5}\left(\frac{1}{5}\kappa_nM\right)I^{(5)}_{\bar{3}\bar{3}}a_3\,,\\\mathscr{F}_{\phi}&=-\frac{2G}{5c^5}\left(\frac{1}{5}\kappa_nM\right)\left[I^{(5)}_{\bar{1}\bar{2}}\cos 2\alpha+(I^{(5)}_{\bar{1}\bar{1}}-I^{(5)}_{\bar{2}\bar{2}})\frac{1}{2}\sin 2\alpha\right](a_1^2-a_2^2)\,,\\\mathscr{F}_{\psi}&=0\,,\\\mathscr{F}_{r}&=-\frac{2G}{5c^5}I^{(5)}_{\bar{1}\bar{1}}\mu r\,,\\\mathscr{F}_{\theta}&=-\frac{2G}{5c^5}I^{(5)}_{\bar{1}\bar{2}}\mu r^2\,.\end{aligned} \tag{9.10}$$

Therefore, the dynamical equations for binaries, equations (5.11)–(5.17), are modified as

$$\ddot{a}_1=\{\cdots\}-\frac{2G}{5c^5}(I^{(5)}_{\bar{1}\bar{1}}\cos^2\alpha+I^{(5)}_{\bar{2}\bar{2}}\sin^2\alpha-I^{(5)}_{\bar{1}\bar{2}}\sin 2\alpha)a_1\,, \tag{9.11}$$

$$\ddot{a}_2=\{\cdots\}-\frac{2G}{5c^5}(I^{(5)}_{\bar{1}\bar{1}}\sin^2\alpha+I^{(5)}_{\bar{2}\bar{2}}\cos^2\alpha+I^{(5)}_{\bar{1}\bar{2}}\sin 2\alpha)a_2\,, \tag{9.12}$$

$$\ddot{a}_3=\{\cdots\}-\frac{2G}{5c^5}I^{(5)}_{\bar{3}\bar{3}}a_3\,, \tag{9.13}$$

$$\frac{d}{dt}(a_1\Omega-a_2\Lambda)=\{\cdots\}-\frac{2G}{5c^5}\left[I^{(5)}_{\bar{1}\bar{2}}\cos 2\alpha+\frac{1}{2}(I^{(5)}_{\bar{1}\bar{1}}-I^{(5)}_{\bar{2}\bar{2}})\sin 2\alpha\right]a_1\,, \tag{9.14}$$

$$\frac{d}{dt}(-a_2\Omega+a_1\Lambda)=\{\cdots\}-\frac{2G}{5c^5}\left[I^{(5)}_{\bar{1}\bar{2}}\cos 2\alpha+\frac{1}{2}(I^{(5)}_{\bar{1}\bar{1}}-I^{(5)}_{\bar{2}\bar{2}})\sin 2\alpha\right]a_2\,, \tag{9.15}$$

$$\ddot{r}=\{\cdots\}-\frac{2G}{5c^5}I^{(5)}_{\bar{1}\bar{1}}r\,, \tag{9.16}$$

$$\ddot{\theta}=\{\cdots\}-\frac{2G}{5c^5}I^{(5)}_{\bar{1}\bar{2}}\,. \tag{9.17}$$

Since $I^{(5)}_{11} + I^{(5)}_{22} + I^{(5)}_{33} = 0$, the expression for $2P_c/\rho_c$ is not affected by the presence of gravitational radiation reaction, i.e., equations (2.30) and (2.34) still apply. Finally, equations (5.18) and (5.19) become

$$\dot{\Omega} = \left(\frac{a_2}{a_1} - \frac{a_1}{a_2}\right)^{-1}\left\{\{\cdots\} + \frac{2G}{5c^5}\left[I^{(5)}_{12}\cos 2\alpha + \frac{1}{2}(I^{(5)}_{11} - I^{(5)}_{22})\sin 2\alpha\right]\left(\frac{a_1}{a_2} + \frac{a_2}{a_1}\right)\right\},$$
$$\dot{\Lambda} = \left(\frac{a_2}{a_1} - \frac{a_1}{a_2}\right)^{-1}\left\{\{\cdots\} + \frac{4G}{5c^5}\left[I^{(5)}_{12}\cos 2\alpha + \frac{1}{2}(I^{(5)}_{11} - I^{(5)}_{22})\sin 2\alpha\right]\right\}. \quad (9.18)$$

Note that the equation $\mathcal{F}_\psi = 0$ again guarantees that the fluid circulation defined by equation (2.13) is conserved.

9.2. *Orbital Decay of Roche-Riemann Binaries*

With the dynamical equations derived in § 9.1 and the expressions for $I^{(5)}_{ij}$ derived in the Appendix, we can now calculate the orbital evolution of a general Roche-Riemann binary driven by the gravitational radiation reaction. In particular, we can study the dynamical behavior of a coalescing neutron star–black hole pair prior to final merging, at least when general relativistic effects are not too important [i.e., when $r_{GR} \sim 6G(M + M')/c^2 < (1 + M'/M)^{1/3}R_0$; see LRS3, § 5].

At large separation, the orbital decay is secular, and the binary evolves along a Roche-Riemann sequence with constant $\mathscr{C}$ (since gravitational radiation reaction forces conserve $\mathscr{C}$). This quasi-static evolution has been discussed extensively in LRS3. At smaller r, when the dynamical stability limit is approached, the dynamical equations must be used. In Figure 12 we show an example of such a dynamical calculation for $p = 1$, $n = 1$, and $R_0 = 5GM/c^2$ (a typical value for neutron stars; see LRS3). The fluid viscosity is assumed to be zero. At $t = 0$, we construct an equilibrium Roche-Riemann configuration with $\mathscr{C} = 0$ and $r/a_1 = 5$. Initially, the binary closely follows the equilibrium constant-$\mathscr{C}$ sequence. As the dynamical instability develops, both the radial velocity and the dynamical tidal lag increase considerably. Thereafter the two stars merge hydrodynamically in just a few orbits (Rasio & Shapiro 1994). This qualitative behavior has already been observed in the simplified calculations we presented in LRS2 and LRS3. The development of a large lag angle is not surprising. It arises because of the finite time necessary for the star to adjust its structure to the rapidly changing tidal potential (cf. Lai 1994a; Lai & Shapiro 1994b).

The small but finite value of α observed in Figure 12 in the limit of large orbital separation can be calculated as follows. Including gravitational radiation reaction, the rate of change of the spin J_s is given by

$$\frac{dJ_s}{dt} = \frac{3GM'}{2r^3}\sin 2\alpha(I_{11} - I_{22}) + \mathcal{F}_\phi, \quad (9.19)$$

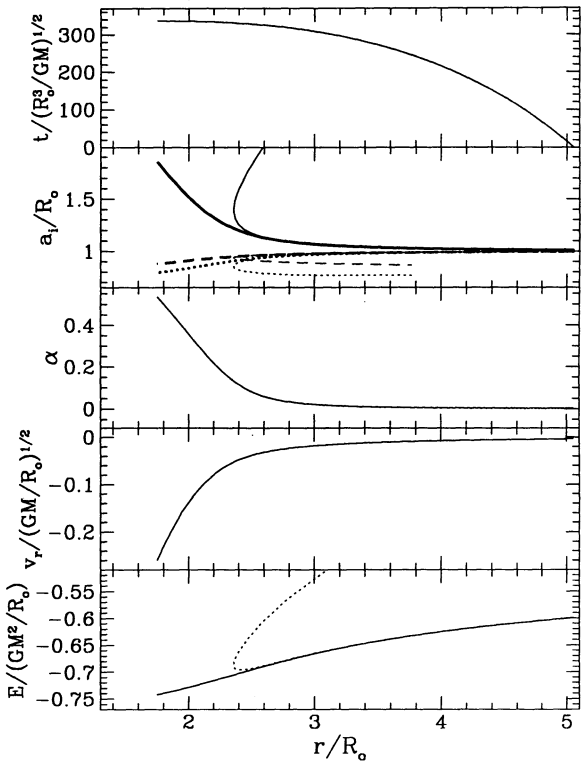

FIG. 12.—Evolution of a Roche-Riemann binary driven by gravitational radiation. Here $p = 1$, $n = 1$, $v = 0$, and $R_0 = 5GM/c^2$. The initial configuration is an equilibrium Roche-Riemann binary with $f_R = -2$ and $r/a_1 = 5$. All quantities are defined as in Fig. 11, and $v_r = \dot{r}$ is the radial velocity. The axes for an equilibrium irrotational Roche-Riemann sequence are shown as lighter lines, while the dynamical values are shown as thicker lines. The total energy for an equilibrium sequence is also shown as a dotted line.

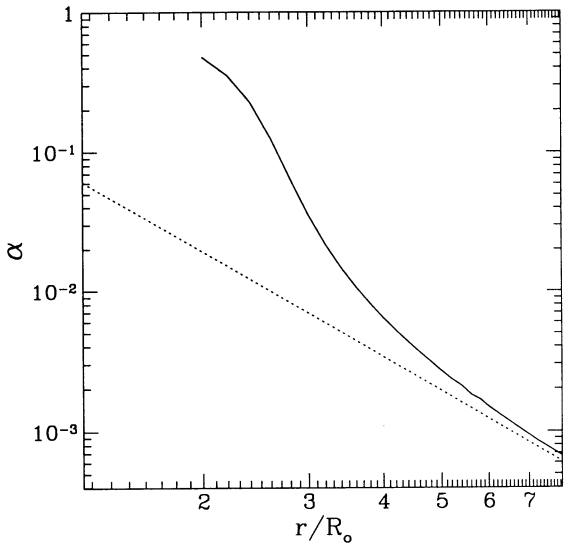

FIG. 13.—Tidal lag angle as a function of binary separation r. Here $p = 1$, $n = 0.5$, and $R_0 = 5GM/c^2$. The solid line is from our dynamical calculation, and the dotted line is an analytic expression for large r (eq. [9.21]).

(see eq. [5.8]), where $\mathscr{F}_\phi$ is given by equation (9.10). Using the expressions derived in the Appendix, we see that the dominant contribution to $\mathscr{F}_\phi$ comes from the terms proportional to $I\!\!I^{(5)}_{12} \simeq 16\Omega^5_{\rm orb}\,\mu r^2$. Thus

$$\frac{dJ_s}{dt} \simeq \frac{3GM'}{2r^3}\sin 2\alpha(I_{11} - I_{22}) - \frac{2G}{5c^5}\left(\frac{1}{5}\kappa_n M\right)(I\!\!I^{(5)}_{12}\cos 2\alpha)(a_1^2 - a_2^2)\,. \tag{9.20}$$

As in § 8.2, consider the limit of large r, so that $J_s \simeq -\mathscr{C}$. Since $d\mathscr{C}/dt = 0$ (cf. eq. [9.10]), we have $dJ_s/dt \simeq 0$. Equation (9.20) then gives

$$\tan 2\alpha \simeq \frac{64}{15}\frac{\Omega^5_{\rm orb}\,G\mu r^2}{c^5 M'} \simeq \frac{64}{15}\left(\frac{GM}{rc^2}\right)^{5/2}\left(1 + \frac{M'}{M}\right)^{3/2}\,. \tag{9.21}$$

Note that this result is independent of the equation of state (the polytropic index n does not appear). In Figure 13, we show the numerical results for α as a function of r. We see that the value of α is indeed given by equation (9.21) where $r/R_0 \gg 1$. However, at smaller separation, for $r/R_0 \lesssim 4$, the lag angle can become considerably larger (by as much as an order of magnitude) than predicted by expression (9.21). This is a result of the dynamical instability.

This work has been supported in part by NSF grant AST 91-19475 and NASA grant NAGW-2364 to Cornell University. Partial support was also provided by a Hubble Fellowship to F. A. R. funded by NASA through grant HF-1037.01-92A from the Space Telescope Science Institute, which is operated by the Association of Universities for Research in Astronomy, Inc., under contract NAS 5-26555. F. A. R. also acknowledges the hospitality of the ITP at the University of California, Santa Barbara.

APPENDIX

EVALUATION OF $I\!\!I^{(5)}_{\bar{i}\bar{j}}$

Consider a triaxial body with its diagonal moment-of-inertia tensor as defined in the body frame given by I_{ij} (eq. [4.20]). We now calculate $I\!\!I^{(5)}_{\bar{i}\bar{j}}$ (cf. eq. [9.2]), the components of $I\!\!I^{(5)}$ projected onto a "projection frame." To define this frame, consider Figure 3, but for now neglect M' by focusing on M: the body coordinates are x_i, and the projection coordinates are $x_{\bar{i}}$, but for now center the projection frame on O. In the special case of a single star, when the projection frame coincides with the body frame, the procedure for calculating $I\!\!I^{(5)}_{\bar{i}\bar{j}}$ has been provided by Miller (1974). Below we generalize this procedure to the case when $\{x_i\}$ and $\{x_{\bar{i}}\}$ are different, as we have for binaries (see § 9).

The coordinates $\{x_i\}$ and $\{x_{\bar{i}}\}$ are related to the inertial coordinates $\{X_i\}$ by

$$x_i = T_{i\alpha}(\phi)X_\alpha\,, \qquad x_{\bar{i}} = T_{\bar{i}\alpha}(\theta)X_\alpha\,, \tag{A1}$$

where

$$\boldsymbol{T}(\phi) = \begin{pmatrix} \cos\phi & \sin\phi & 0 \\ -\sin\phi & \cos\phi & 0 \\ 0 & 0 & 1 \end{pmatrix}, \tag{A2}$$

and similarly for $\boldsymbol{T}(\theta)$. The components of the reduced quadrupole tensor in the inertial frame are

$$\mathcal{I}^{(\mathrm{in})}_{\alpha\beta} = T^{\dagger}_{\alpha k}(\phi) T^{\dagger}_{\beta l}(\phi) \mathcal{I}_{kl} \,. \tag{A3}$$

Thus we have

$$\begin{aligned} \mathcal{I}^{(5)}_{\bar{i}\,\bar{j}} &= T_{\bar{i}\alpha}(\theta) T_{\bar{j}\beta}(\theta) \frac{d^5}{dt^5} \left[T^{\dagger}_{\alpha k}(\phi) T^{\dagger}_{\beta l}(\phi) \mathcal{I}_{kl} \right] \\ &= \sum_{m=0}^{5} C^5_m \left(\frac{d^{5-m}}{dt^{5-m}} \mathcal{I}_{kl} \right) T_{\bar{i}\alpha}(\theta) T_{\bar{j}\beta}(\theta) \frac{d^m}{dt^m} \left[T^{\dagger}_{\alpha k}(\phi) T^{\dagger}_{\beta l}(\phi) \right] \\ &= \sum_{m=0}^{5} C^5_m \left(\frac{d^{5-m}}{dt^{5-m}} \mathcal{I}_{kl} \right) \sum_{p=0}^{m} C^m_p R^p_{\bar{i}k} R^{m-p}_{\bar{j}l} \,, \end{aligned} \tag{A4}$$

where the constants C^5_m are binomial coefficients, and

$$R^p_{\bar{i}k} = T_{\bar{i}\alpha}(\theta) \frac{d^p}{dt^p} T^{\dagger}_{\alpha k}(\phi) \,. \tag{A5}$$

In general, equations (A4) and (A5) are complicated to evaluate. In the quasi-static limit, when $|da_i/dt| \ll |\Omega a_i|$, simple expressions for $\mathcal{I}^{(5)}_{ij}$ can be derived. To lowest order in da_i/dt, we have

$$\mathcal{I}^{(5)}_{\bar{i}\,\bar{j}} \simeq \sum_k I_{kk} \sum_{p=0}^{5} C^5_p R^p_{\bar{i}k} R^{5-p}_{\bar{j}k} + 5 \sum_k \dot{I}_{kk} \sum_{p=0}^{4} C^4_p R^p_{\bar{i}k} R^{5-p}_{\bar{j}k} \,, \tag{A6}$$

where we have used

$$\mathcal{I}^{(\mathrm{in})}_{\alpha\beta} = T^{\dagger}_{\alpha k}(\phi) T^{\dagger}_{\beta l}(\phi) I_{kl} - \tfrac{1}{3} I_{kk} \delta_{\alpha\beta} \tag{A7}$$

and $dI_{kk}/dt \simeq 0$ in the quasi-static approximation.

The matrix R^p can now be evaluated, keeping terms up to order $\dot{\Omega}$. After some algebra, we obtain

$$[\mathcal{I}^{(5)}_{\bar{i}\,\bar{j}}] = 16\Omega^5 (I_{11} - I_{22}) \begin{pmatrix} \sin 2\alpha & \cos 2\alpha & 0 \\ \cos 2\alpha & -\sin 2\alpha & 0 \\ 0 & 0 & 0 \end{pmatrix} + 40\Omega^3 [\Omega(\dot{I}_{11} - \dot{I}_{22}) + 2\dot{\Omega}(I_{11} - I_{22})] \begin{pmatrix} \cos 2\alpha & -\sin 2\alpha & 0 \\ -\sin 2\alpha & -\cos 2\alpha & 0 \\ 0 & 0 & 0 \end{pmatrix} . \tag{A8}$$

We can now write down the components $\mathcal{I}^{(5)}_{\bar{i}\,\bar{j}}$ that appear in our dynamical equations. For the single-star case, the projection frame coincides with the body frame. Setting $\alpha = 0$ in equation (A8), we see that the only components are

$$\mathcal{I}^{(5)}_{11} = -\mathcal{I}^{(5)}_{22} = 40\Omega^3 [\Omega(\dot{I}_{11} - \dot{I}_{22}) + 2\dot{\Omega}(I_{11} - I_{22})] \,, \qquad \mathcal{I}^{(5)}_{12} = \mathcal{I}^{(5)}_{21} = 16\Omega^5 (I_{11} - I_{22}) \,, \tag{A9}$$

where the I_{ii} are defined in equation (4.20).

To evaluate $\mathcal{I}^{(5)}_{\bar{i}\,\bar{j}}$ for a Roche-Riemann binary, we now move the origin of the projection coordinates $\{x_{\bar{i}}\}$ back to the system CM as in Figure 3 and equation (9.1). But then we can decompose the total moment of inertia into two contributions: the orbital part due to two point masses M and M', and the fluid part due to the ellipsoid M. The contribution from the ellipsoid is given by equation (A8). The resulting nonzero components of $\mathcal{I}^{(5)}_{\bar{i}\,\bar{j}}$ are

$$\begin{aligned} \mathcal{I}^{(5)}_{\bar{1}\bar{1}} &= -\mathcal{I}^{(5)}_{\bar{2}\bar{2}} = 16\Omega^5 (I_{11} - I_{22}) \sin 2\alpha + 40\Omega^3_{\mathrm{orb}} [2\Omega_{\mathrm{orb}} \mu r \dot{r} + 2\dot{\Omega}_{\mathrm{orb}} \mu r^2] + 40\Omega^3 [\Omega(\dot{I}_{11} - \dot{I}_{22}) + 2\dot{\Omega}(I_{11} - I_{22})] \cos 2\alpha \,, \\ \mathcal{I}^{(5)}_{\bar{1}\bar{2}} &= \mathcal{I}^{(5)}_{\bar{2}\bar{1}} = 16\Omega^5_{\mathrm{orb}} \mu r^2 + 16\Omega^5 (I_{11} - I_{22}) \cos 2\alpha - 40\Omega^3 [\Omega(\dot{I}_{11} - \dot{I}_{22}) + 2\dot{\Omega}(I_{11} - I_{22})] \sin 2\alpha \,. \end{aligned} \tag{A10}$$

These expressions obviously do not apply to certain dynamical situations, such as the hyperbolic fly-by of a star past a black hole. In such a case the variables r and a_i change rapidly, and higher order time derivatives must be retained. For two point masses, the expressions for $\mathcal{I}^{(5)}_{\bar{i}\,\bar{j}}$ can be evaluated analytically with repeated use of the equation of motion.

REFERENCES

Abramovici, A., et al. 1992, Science, 256, 325
Aizenman, M. L. 1968, ApJ, 153, 511
Boss, A. P., Cameron, A. G. W., & Benz, W. 1991, Icarus, 92, 165
Carter, B., & Luminet, J. P. 1983, A&A, 121, 97
———. 1985, MNRAS, 212, 23
Chandrasekhar, S. 1961, Hydrodynamics and Hydromagnetic Stability (Oxford: Oxford Univ. Press)
———. 1969, Ellipsoidal Figures of Equilibrium (New Haven: Yale Univ. Press) (Ch69)
———. 1970, ApJ, 161, 561
Cox, J. P. 1980, Theory of Stellar Pulsation (Princeton: Princeton Univ. Press)
Detweiler, S. L., & Lindblom, L. 1977, ApJ, 213, 193
Eichler, D., Livio, M., Piran, T., & Schramm, D. N. 1989, Nature, 340, 126
Evans, C. R., Iben, I., & Smarr, L. 1987, ApJ, 323, 129
Evans, C. R., & Kochanek, C. S. 1989, ApJ, 346, L13
Fabian, A. C., Pringle, J. E., & Rees, M. J. 1975, MNRAS, 172, 15P
Goldreich, P., & Peale, S. J. 1968, ARA&A, 6, 287
Goldstein, H. 1980, Classical Mechanics (Reading: Addison-Wesley)
Ipser, J., & Managan, M. 1981, ApJ, 256, 145
Kochanek, C. S. 1992a, ApJ, 385, 604
———. 1992b, ApJ, 398, 234
Kosovichev, A. G., & Novikov, I. D. 1992, MNRAS, 258, 715
Laguna, P., Miller, W. A., Zurek, W. H., & Davies, M. B. 1993, ApJ, 410, L83
Lai, D. 1994a, MNRAS, in press

Lai, D. 1994b, Ph.D. thesis, Cornell Univ.
Lai, D., Rasio, F. A., & Shapiro, S. L. 1993a, ApJS, 88, 205 (LRS1)
———. 1993b, ApJ, 406, L63 (LRS2)
———. 1993c, ApJ, 412, 593
———. 1994a, ApJ, 420, 811 (LRS3)
———. 1994b, ApJ, 423, 344 (LRS4)
Lai, D., & Shapiro, S. L. 1994a, ApJ, submitted
———. 1994b, ApJ, submitted
Landau, L. D., & Lifshitz, E. M. 1987, Fluid Mechanics (2d ed.; Oxford: Pergamon)
Lebovitz, N. R. 1966, ApJ, 145, 878
Lee, H. M., & Ostriker, J. P. 1986, ApJ, 310, 176
Lindblom, L., & Detweiler, S. L. 1977, ApJ, 211, 565
Luminet, J. P., & Carter, B. 1986, ApJS, 61, 219
McMillan, S. L. W., McDermott, P. N., & Taam, R. E. 1987, ApJ, 318, 261
Miller, B. D. 1974, ApJ, 187, 609
Misner, C. M., Thorne, K. S., & Wheeler, J. A. 1973, Gravitation (San Francisco: Freeman)
Nduka, A. 1971, ApJ, 170, 131
Novikov, I. D., Pethick, C. J., & Polnarev, A. G. 1992, MNRAS, 255, 276
Paczyński, B. 1986, ApJ, 308, L43
Press, W. H., & Teukolsky, S. A. 1973, ApJ, 181, 513
———. 1977, ApJ, 213, 183 (PT)
Press, W. H., Teukolsky, S. A., Vetterling, W. T., & Flannery, B. P. 1992, Numerical Recipes: The Art of Scientific Computing (2d ed.; Cambridge: Cambridge Univ. Press)
Rasio, F. A. 1993, PASP, 105, 973
Rasio, F. A., & Shapiro, S. L. 1991, ApJ, 377, 559
———. 1994, ApJ, 432, 242
Rees, M. J. 1988, Nature, 333, 523
Roberts, P. H., & Stewartson, K. 1963, ApJ, 137, 777
Rossner, L. F. 1967, ApJ, 149, 145
Shapiro, S. L. 1979, in Sources of Gravitational Radiation, ed. L. Smarr (Cambridge: Cambridge Univ. Press), 355
Sridhar, S., & Tremaine, S. 1992, Icarus, 95, 86
Tassoul, J.-L. 1970, ApJ, 160, 1031
———. 1978, Theory of Rotating Stars (Princeton: Princeton Univ. Press)
Yungelson, L. R., Livio, M., Tutukov, A. V., & Saffer, R. A. 1994, ApJ, 420, 336
Zahn, J. P. 1970, A&A, 4, 452